ACS OMEGA

Open Access

http://pubs.acs.org/journal/acsodf

Article

Synergistic Treatment of Breast Cancer by Combining the Antimicrobial Peptide Piscidin with a Modified Glycolipid

Rebecca T. Miceli, Noah G. Allen, Bhagyashree Subramaniam, Livia Carmody, Jonathan S. Dordick, David T. Corr, Myriam Cotten,* and Richard A. Gross*

Cite This: *ACS Omega* 2024, 9, 33408−33424

Read Online

ACCESS | Metrics & More | Article Recommendations | Supporting Information

ABSTRACT: Piscidin 3 (P3), a peptide produced by fish, and a hexyl ester-modified sophorolipid (SL-HE), have individually shown promise as antimicrobial and anticancer drugs. A recent report by our team revealed that combining P3 with SL-HE in a 1:8 molar ratio resulted in an 8-fold enhancement in peptide activity, while SL-HE improved by 25-fold its antimicrobial activity against the Gram-positive microorganism *Bacillus cereus*. Extending these findings, the same P3/SL-HE combination was assessed on two breast cancer cell lines: BT-474, a hormonally positive cell line, and MDA-MB-231, an aggressive triple-negative cell line. The results demonstrated that the 1:8 molar ratio of P3/SL-HE synergistically enhances the anticancer effects against both tumorigenic breast cell lines. Mechanistic studies indicate the activation of an intrinsic apoptotic cell death mechanism through an increase in reactive oxygen species and mitochondrial dysfunction and a secondary programmed necrotic pathway that involves pore formation in the plasma membrane. When a fibroblast cell line, CCD1065SK HDF, was utilized to determine selectivity, the synergistic SL-HE/P3 combination exhibited a protective property compared to the use of SL-HE alone and therefore afforded vastly improved selectivity indices. Given the promising results reported herein, the synergistic combination of P3/SL-HE constitutes a novel strategy that merits further study for the treatment of breast cancer.

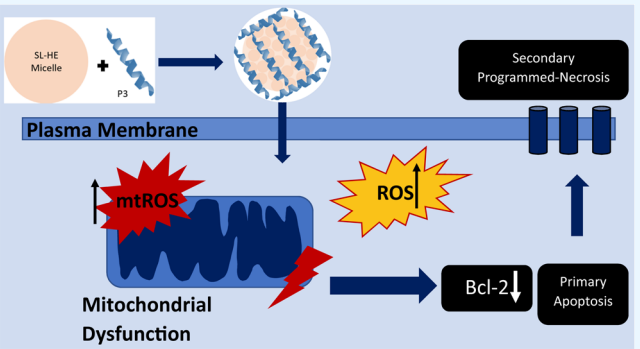

INTRODUCTION

Increased knowledge about mechanisms of anticancer drug activity has opened new avenues to the rational development of synergistic drug combinations.[1−4] The combined effect of multiple drugs to treat a disease can be organized into three categories: additive (or noninteractive), antagonistic, and synergistic.[1] Although the term "synergy" is often misused to represent the combined effects of two compounds,[5] in truly synergistic drug combinations (drug potentiation), the effect of two drugs in combination is more biologically potent than expected from their additive effects.[1,6,7] These synergistic drug combinations represent an important strategy to improve the therapeutic efficacy of a drug while reducing harsh adverse side effects.[8] There is a current lack of knowledge on how synergistic drug combinations function to enhance their therapeutic efficacy. In this study, we combined two different classes of biomolecules, a peptide and a glycolipid, to effectuate synergistic anticancer activity.

First discovered for its antimicrobial activity, P3 (FIHHIFR-GIVHAGRSIGRFLTG), a host defense peptide expressed in hybrid striped bass, is also active on cancer cells.[9−14] Unstructured in buffer, P3 adopts an amphipathic α-helical conformation in the presence of lipid membranes and DNA.[10] Against bacterial strains, P3 acts through multiple modes of action, including the formation of transient defects and pores in membranes and colocalization with DNA inside the cell, causing charge neutralization and aggregation of nucleic acids.[13,15−17] P3 is moderately active on various cancer cell lines, including triple-negative breast (MDA-MB-231) (IC_{50} = 17.5 ± 8.5 μM), fibrosarcoma (HT1080) (IC_{50} = 26.01 ± 2.6 μM), and lung (A549) (IC_{50} = 21.6 ± 1.2 μM) cancer cells.[13] A homologue, tilapia P3 (TP3), has shown anticancer activity on osteosarcoma cells (IC_{50} = 10.0 ± 1.10 μM)[9] and glioblastoma cells (significant changes to filopodia at 1 μM).[18]

Sophorolipids (SLs) are natural glycolipid biosurfactants produced in high volumetric titers (~200 g/L) from the nonpathogenic yeast *Starmerella bombicola*.[19,20] SL esters are a versatile family of synthetically modified SLs.[20−28] They are synthesized by an alcoholysis reaction between natural diacetylated lactonic sophorolipid (DLSL) and an alcohol under alkaline conditions.[29,30] Of particular interest herein is

Received: December 11, 2023
Revised: April 30, 2024
Accepted: June 11, 2024
Published: July 24, 2024

https://doi.org/10.1021/acsomega.3c09902
ACS Omega 2024, 9, 33408−33424

SL-HE (Figure 1), where the primary alcohol used is *n*-hexanol, and a concurrent deacetylation of sophorose occurs due to alkaline reaction conditions.[31]

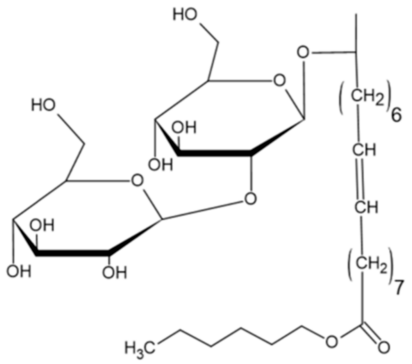

Figure 1. Sophorolipid hexyl ester.

SLs possess many biological properties, including anticancer,[27,28,32−35] anti-inflammatory,[24,36−38] antisepsis,[37,39] and immunomodulatory activities.[36] The literature on SLs indicates that DLSL can induce increased reactive oxygen species (ROS) on MDA-MB-231 cells,[34] as well as apoptosis in ovarian (HeLa) tumorigenic cells, through activation of an ER-mediated pathway.[40] The sophorolipid analogues SL-methyl and SL-ethyl ester were reported to cause pancreatic cancer cell cancer death by a necrotic pathway.[41] We recently reported a study in which cultured MDA-MB-231 breast cancer cells were dosed individually with DLSL (IC_{50} = 20 μM) and diacetylated SL ethyl ester (SL-EE-D) (IC_{50} = 33 μM).[27] These results highlight that natural and modified SLs can provide anticancer activity. Here, we describe how antagonistic interactions can be used to reduce the cytotoxicity of an SL ester toward a nontumorigenic cell line while increasing its activity toward cancer cell lines.

Fortuitously, our team discovered through a series of biophysical studies that SL-HE and P3 form aggregates through noncovalent interactions.[42] These studies reveal four key features: (1) P3 binds to SL-HE aggregates, becoming α-helical; (2) piscidin−glycolipid assemblies synergistically accumulate on membranes; (3) defects in phospholipid bilayers are induced by SL-HE alone or bound to P3; (4) disruption of the bilayer structure occurs differently and to a greater extent in the presence of piscidin−glycolipid complexes than when incubated with either compound alone.[42] The cumulative results of this work led to the hypothesis that interactions between SL-HE and P3 result in a prefolding of the peptide that potentiates delivery of both agents to bacterial surfaces resulting in membrane disruption. Given that SLs are ubiquitously and safely used in consumer products,[20,26,28,31,43] the biophysical characteristics of SL/peptide are of interest for other therapeutic functions.

The current study seeks to expand on the biophysical and antimicrobial studies described above. The combination of P3/SL-HE in a 1:8 molar ratio was explored whether the aggregate structure formed would synergistically increase the cytotoxicity and selectivity when used to treat tumorigenic breast cell lines, MDA-MB-231 and BT-474, as well as the nontumorigenic human dermal fibroblast (HDF) cell line CCD1065SK HDF. We first determined dose−response effects for SL-HE, P3, and their combination in a fixed 1:8 molar ratio and then analyzed a mechanism of action for the combined drug against tumorigenic cell lines. The results are discussed in the context of previous studies published on the anticancer effects of P3 and SLs. We highlight possible future routes of future investigations.

RESULTS

Prior Characterization of the P3 and SL-HE Complex.

The rationale for the study herein is based on a recent investigation by our group, Liu et al., 2023, where the combination of either P3 or its homologue piscidin 1 (P1) with SL-HE used at a 1:8 molar ratio acted synergistically against the Gram-positive microorganism *Bacillus cereus*.[42] Using submicromolar concentrations of P3 resulted in 8-fold improvement in peptide activity, while SL-HE experienced a 25-fold enhancement. Permeabilization assays and biophysical studies in a 1:8 molar ratio were conducted to determine the key underlying features that result in strong synergistic antimicrobial activity against *B. cereus*.[42] These studies revealed that the micelles formed by SL-HE provide a surface for P3 to bind and fold into an α-helix. The SL-HE micelles loaded with piscidin can then deliver large amounts of peptide to bacterial cell membranes, leading to major membrane disruption as the membrane-active peptide and glycolipid insert into the

Table 1. Apparent IC_{50} and FIC Values for P3 Singly, SL-HE Singly, and P3/SL-HE in a 1:8 molar Combination against MDA-MB-231, BT-474, and CCD1065SK HDF Cells[a]

cell line	agent	apparent IC_{50}, singly (μM)[b]	apparent IC_{50}, in combination (μM)[c]	FIC[d]	outcome
MDA-MB-231	P3	66	7.5	0.83	synergy
	SL-HE	83	60		
	DOX	15[46]			
BT-474	P3	66	2.7	0.38	synergy
	SL-HE	65	22		
	DOX	1.1[47]			
CCD1065SK HDF	P3	>66	24	22	antagonism
	SL-HE	8.7	192		
	DOX	53[27]			

[a]Comparison against the gold standard chemotherapeutic doxorubicin (DOX) included for reference. [b]Footnote: IC_{50} was determined using GraphPad Prism10. Absolute IC_{50} function, where dose−response curves for SL-HE singly and P3 singly are displayed in Figure S1, and the combined dose−response curves are displayed in Figure 2. [c]Combined IC_{50} indicates that for every 1 M P3, there is a corresponding 8 M SL−HE in a mixture. [d]FIC was determined according to eq 1 (see Materials and Methods), where FIC < 1 indicates synergy and FIC > 1 indicates antagonism.

https://doi.org/10.1021/acsomega.3c09902
ACS Omega 2024, 9, 33408−33424

membrane, with the glycolipid promoting enhanced membrane accumulation of the peptide. Permeabilization assays and biophysical studies including surface plasmon resonance, circular dichroism, NMR, mass spectrometry, and X-ray diffraction revealed four key mechanistic features underlying a synergistic action on microbial membranes.[42] The findings included the following: (1) P3 binds to SL-HE aggregates, resulting in a α-helical conformation; (2) the P3/SL-HE combined drug synergistically accumulates on membranes; (3) SL-HE induces defects upon association with phospholipid bilayers either alone or bound to P3; and (4) the P3/SL-HE complex can disrupt the bilayer structure more efficiently and differently than either compound alone.[42] Our team has applied our knowledge for the biophysical associations of P3/SL-HE in a 1:8 molar ratio against bacterial membranes to its use as a novel anticancer therapeutic against two different breast cancer cell lines, the less aggressive, triple-positive BT-474 cells and the more aggressive, harder-to-treat triple-negative cell line MDA-MB-231.

Synergistic Effect and Dose−Response Curves of Combined P3 and SL-HE. To investigate the biological activity of P3 and SL-HE singly and combined at a 1:8 molar ratio, apparent half-maximal inhibitory concentration (IC_{50}) values and fractional inhibitory concentrations (FICs) were obtained on three cell lines (Table 1, Figure 2). The term

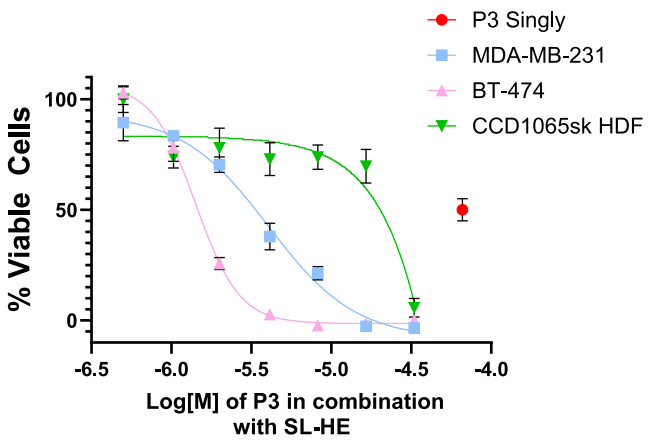

Figure 2. Dose−response assay for MDA-MB-231, BT-474, and CCD1065SK HDF cells of P3 in a P3/SL-HE mixture (1:8 molar ratio). P3 singly (red) indicates an apparent 50% cell death for tumorigenic cells. Absolute IC_{50} values, calculated with GraphPad Prism10, are given in Table 1. n = 3/dose. Note that some error bars are too small to be seen within the graph.

apparent IC_{50} is utilized due to the methods in which the synergy combination, where we assume a 1:8 molar ratio exists throughout the dilution process. A tetrazolium-based assay optimized for monolayer cell culture was used to obtain dose−response cell viability curves.[44,45] Positive and negative controls were performed using untreated cells and media only wells, respectively. To determine synergy, we calculated FICs, see eq 1 in Materials and Methods.

Due to the limited solubility of P3 and its low activity on all cell lines, full dose−response curves could not be obtained. While no cell death was reported up to 33 μM, a concentration corresponding to approximately 50% cell death occurred at 66 μM for both tumorigenic MDA-MB-231 (Figure S1A) and BT-474 cells and at >66 μM for nontumorigenic HDF cells. To achieve the 66 μM concentration, 20% of cell media was replaced by the peptide, compared to 10% replacement for the lower-peptide concentrations, as explained in the Materials and Methods section.

Incubation of SL-HE singly and P3 singly (Figure S1) against the aggressive MDA-MB-231 breast cancer cell line for 24 h resulted in dose-dependent cell death with an IC_{50} value of 83 μM SL-HE (Table 1). The 1:8 molar ratio of P3/SL-HE resulted in a 9-fold drop in the apparent IC_{50} of P3, from 66 to 7.5 μM (Figure 2, Table 1). The resulting apparent FIC value is 0.83, indicating a weakly synergistic drug combination. The BT-474 tumorigenic cell line is triple-positive for ER, PR, and HER2 and is typically regarded as less aggressive, less metastatic, and easier to treat, respectively. The dose−response curve (Figure S1B) and the resulting IC_{50} value of SL-HE singly on this cell line is 65 μM (Table 1). The mixture of P3/SL-HE in a 1:8 molar ratio resulted in a 24-fold drop in the P3 concentration needed to decrease the apparent IC_{50} from 66 to 2.7 μM (Figure 2, Table 1). The resulting apparent FIC value is 0.38, which indicates a strong synergistic combination of the two drugs. Thus, the presence of SL-HE improves the activity of P3 against BT-474 tumorigenic cells.

The nontumorigenic breast-derived human dermal fibroblast cell line CCD1065SK was utilized to determine selectivity indices. The dose−response curve and the resulting IC_{50} value for SL-HE singly against HDF cells was 8.7 μM, representing higher cytotoxicity to nontumorigenic cells compared with tumorigenic cells (Figure S1, Table 1). When the HDF cells were dosed with the P3/SL-HE mixture (1:8 molar ratio), the apparent IC_{50} value of P3 increased to 24 μM (Figure 2, Table 1). In other words, addition of SL-HE to P3 resulted in about a 3-fold increase in P3 cytotoxicity. Furthermore, at the P3/SL-HE mixture, the concentrations of SL-HE and P3 at the IC_{50} for HDF cells was 24 μM and 192 μM, respectively (Table 1). Hence, the cytotoxicity of SL-HE decreased 22-fold compared to SL-HE singly by its combination with P3. Accordingly, P3 protects HDF cells from SL-HE, which when present singly exhibit a much higher toxicity. The apparent FIC for HDF cells is 22, which indicates antagonism between the two drugs in combination.

Additionally, apparent IC_{50} values from a gold standard chemotherapeutic, doxorubicin (DOX), are shown as a reference comparison to P3, SL-HE, and the combined drug. While DOX dosed singly against MDA-MB-231 and BT-474 tumorigenic cell lines is more potent than either P3 or SL-HE singly, it is similar to the IC_{50} of P3 when dosed in combination with SL-HE at a 1:8 molar ratio (e.g., MDA-MB-231 cells, DOX IC_{50} of 15 μM compared to P3 (in combination with SL-HE) of IC_{50} of 7.5 μM). Additionally, a review by our team showed that reported IC_{50} values of DOX against different cancerous cell lines vary significantly.[48]

Selectivity of P3, SL-HE, and Synergistic Combination toward Cancer Cell Lines. The apparent selectivity index (SI) was determined by calculating the ratio of the median lethal dose (LD_{50}) to the median effective/therapeutic dose (ED_{50}) of a given substance. See eq 2 in Materials and Methods.

The nontumorigenic fibroblast cell line IC_{50} was used as the LD_{50}, while the IC_{50} of the given drug against the tumorigenic cells was used as the ED_{50}. Generally, SI $\geq$ 3 has been used as a criterion warranting further studies for anticancer therapeutic development.[49] The corresponding SI values indicate that SL-HE singly has a higher selectivity for nontumorigenic cells compared with tumorigenic cells, as the SI values for both

https://doi.org/10.1021/acsomega.3c09902
ACS Omega 2024, 9, 33408−33424

cancer cell lines are under 1. SI for P3 singly was not calculated due to very weak activity of the peptide on the tumorigenic and nontumorigenic cells (IC_{50} > 50 μM). Hence, it is noted as N/A in Table 2. The apparent SI values of the IC_{50} values

Table 2. SI Values Determined by Cytotoxicity Values for the Tumorigenic Cell Lines MDA-MB-231 and BT-474 Compared to the Cytotoxicity against Non-tumorigenic CCD1065SK HDF Cells

cell line	agent	apparent SI of drugs singly[a]	apparent SI in combination drug[b]
MDA-MB-231	P3	N/A	3.2
	SL-HE	0.11	
BT-474	P3	N/A	8.9
	SL-HE	0.13	

[a]Footnote: SI was calculated according to eq 2. [b]Apparent IC_{50} was used to calculate the SI from the combined drug (i.e., MDA-MB-231 SI = 24/7.5 and BT-474 SI = 24/2.7).

resulting from dosing with the P3/SL-HE mixture (1:8 molar ratio) are 3.2 and 8.9 against MDA-MB-231 and BT-474 cells, respectively (Table 2). Results indicate that the addition of SL-HE to P3 improves the SI compared to SL-HE singly.

Intracellular Reactive Oxygen Species and Mitochondrial Superoxide Levels. Intracellular ROS are a group of highly reactive molecules that are involved in and affected by many cellular signaling pathways.[50−55] Tumorigenic cell lines typically have increased levels of ROS compared to nontumorigenic cell lines due to gene mutations, increased metabolism, and a more hypoxic microenvironment.[54] The increased ROS levels in tumorigenic cells are regulated by excess antioxidant behavior. Hydrogen peroxide (H_2O_2) or superoxide radicals ($O_2^{\bullet-}$) are the main intracellular ROS species. The production of ROS in the endoplasmic reticulum (ER) has been linked to stress and the unfolded protein response. In other words, when the ER-stress becomes severe, the unfolded protein response is genetically or chemically impaired.[56] Three types of programmed cell death can be induced by excess ROS: apoptosis, programmed necrosis, and autophagy.[50−52]

Herein, cellular oxidative stress was measured using CellROX and flow cytometry for high-throughput quantification of both MDA-MB-231 and BT-474 cell lines following 24 h exposure to the P3/SL-HE mixture. The positive control throughout the mitochondrial dysfunction and CellROX experiments was 50% DMSO, which induces significant cell death in the given time frame. Median fluorescence intensity was used to measure intracellular production of ROS in response to treatment (Figure S2). Similarly, MitoSOX staining with flow cytometry was used to quantify mitochondrial superoxide production in both cell lines during 9 h time course experiments. Median fluorescence intensity was used to detect changes in mitochondrial superoxide production (Figure S2). After exposure of each cell line to the combined drug at the corresponding apparent IC_{50} value, both intracellular and mitochondrial ROS were elevated in MDA-MB-231 cells, while only intracellular ROS was elevated for BT-474 cells. For MDA-MB-231 tumorigenic cells, modest but statistically significant increases in both intracellular ROS after a 24 h incubation (Figure 3A) and mitochondrial superoxide after a 9 h incubation (Figure 3B) were detected. For BT-474 tumorigenic cells, modest but statistically

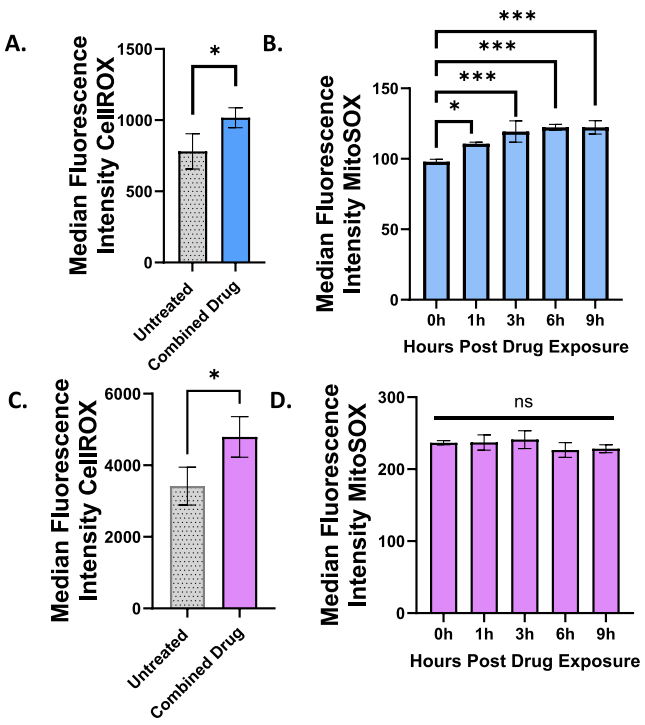

Figure 3. Intracellular reactive oxygen species and mitochondrial superoxide levels after combined drug treatment in tumorigenic cells. The MDA-MB-231 cell line is represented in blue and BT-474 cell line in purple. Median ROS in MDA-MB-231 cells at 24 h postdrug administration (A) and median mitochondrial superoxide content in MDA-MB-231 from 0 to 9 h (B). Median intracellular ROS positivity in BT-474 cells at 24 h postdrug administration (C) and median mitochondrial superoxide content in BT-474 cells from 0 to 9 h postdrug administration (D). The combination drug concentration was at the IC_{50}, determined for each respective cell line. Statistics were calculated in GraphPad Prism10, Students *t*-test was applied for 24 h intracellular ROS (A,C), and one-way ANOVA was applied for mitochondrial superoxide with Tukey's test for multiple comparisons represented (B and D). *p < 0.05, and ***p < 0.001.

significant increases in intracellular ROS after a 24 h incubation occurred (Figure 3C), whereas, the 9 h exposure did not result in any notable change in mitochondrial superoxide generation (Figure 3D). Additionally, intracellular ROS levels (Figure S3) and mitochondrial superoxide (Figure S4) for P3 singly and SL-HE singly are shown, where P3 singly resulted in a strong decrease in intracellular ROS for MDA-MB-231 cells and no change for BT-474 cells. Dosing with SL-HE singly resulted in a pronounced increase in intracellular ROS in both cell lines. In the mitochondrial superoxide assay, there were no significant differences upon adding SL-HE. These results may indicate that SL-HE alone drives an increase in cell stress that is sufficient to overcome the opposite effect from P3. Since a higher content of ROS can cause cell death by processes such as apoptosis, necrosis, and autophagy, further investigation of cell death pathways using mitochondrial dysfunction and protein activity assays were performed and discussed below.

Mitochondrial Dysfunction. Mitochondria are highly dynamic organelles that produce cellular adenosine triphosphate (ATP) as the primary energy source for most physiological and biochemical processes, such as growth, movement, and homeostasis.[57] Mitochondria are also important regulators of several metabolic pathways, including

https://doi.org/10.1021/acsomega.3c09902
ACS Omega 2024, 9, 33408−33424

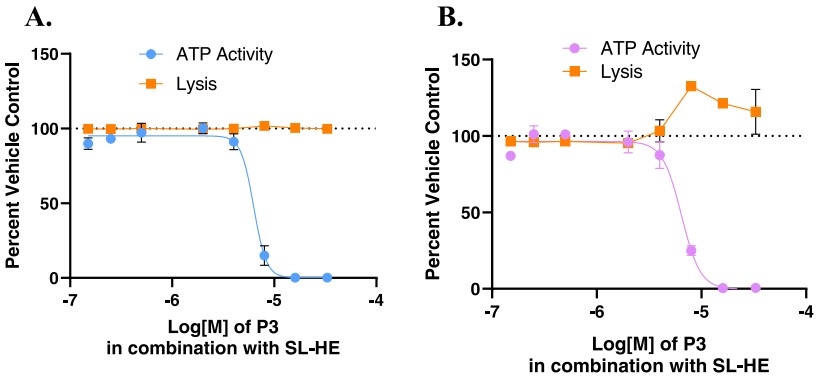

Figure 4. Mitochondrial dysfunction from combined drug exposure on tumorigenic cell lines. Analysis of the P3/SL-HE combination drug on mitochondrial dysfunction for MDA-MB-231 in blue (A) and BT-474 in purple (B), after a 90 min exposure period. Results indicate that the 1:8 P3/SL-HE mixture induces mitochondrial dysfunction on both tumorigenic cell lines due to the decrease in intracellular ATP, with no lysis (orange) observed for MDA-MB-231 and low levels of BT-474 lysis. The untreated control cells consisting of 100% vehicle are displayed as horizontal dotted lines. Note that some error bars are too small to be seen within the graph.

apoptosis and ROS consumption and production.[57] Mitochondrial dysfunction is closely interconnected with the regulation of the Bcl-2 pro-apoptotic protein family. Mitochondrial fission, membrane depolarization, cytochrome *c* release, and mitochondrial pore formation can result from the down-regulation of Bcl-2 and the subsequent upregulation of proapoptotic proteins such as Bax and Bak which act directly on the mitochondria.[58,59]

A multiplex mitochondrial dysfunction assay was used to investigate the changes in intracellular ATP levels and cell death by plasma membrane lysis that are induced upon adding the combined drugs to MDA-MB-231 (Figure 4A) and BT-474 (Figure 4B) tumorigenic cells. A short-course drug exposure of only 90 min resulted in a stark decrease down to zero in intracellular ATP levels for both cell lines. No cell membrane lysis was observed for MDA-MB-231 cells. However, approximately 25% increase in cell lysis was recorded for BT-474 cells dosed with ∼8, 16, and 33 μM P3 combined with SL-HE (1:8 molar ratio). These data indicate that the BT-474 cells are more susceptible to cell lysis than MDA-MB-231 cells. Such differences in cell lysis upon treatment with the combined drug are likely a consequence of the substantial differences in BT-474 and MDA-MB-231 plasma membrane compositions.[60] For instance, PC, cholesterol, monoacylglycerols, diacylglycerols, and fatty acid concentrations are the largest sources of variance between triple-negative and triple-positive hormonal breast cancer cells, where BT-474 cells generally have increased amounts of these membrane components compared to MDA-MB-231 cells.[61] Recently, ATP-targeting drugs have been found to reduce cancer cell growth and disrupt the plasma membrane, thus a chemotherapeutic that targets ATP could be a highly efficient killer of cancer cells.[62] Additionally, the reduction of ATP levels can enhance anticancer drug sensitivity and reduce a possible immune response from the introduction of additional chemotherapeutics.[62] Since mitochondrial dysfunction can be related to apoptosis, programmed necrosis, and autophagy, we next used an Annexin V assay to analyze translocation of phosphatidylserine (PS) to the outer plasma membrane and performed protein assays provided to help differentiate apoptosis, autophagy, and necrotic-like pathways.

Annexin V for Translocation of Phosphatidylserine. The plasma membrane of tumorigenic cells typically exhibits phospholipid asymmetry. In normal cells, phosphatidylcholine (PC) and sphingomyelin are more predominately located on the outer leaflet, and phosphatidylethanolamine (PE) and phosphatidylserine (PS) are located on the inner leaflet of the plasma membrane.[63] It is largely accepted that cells undergoing apoptosis experience a plasma membrane rearrangement in which PS is translocated to the outer leaflet. Annexin V is an anticoagulant that binds to PS, thereby providing a tool to distinguish apoptosis from necrosis.[64−66] Recently, multiple modes of cell death, including primary necrosis,[66,67] necroptosis,[68,69] pyroptosis,[69] and ferroptosis,[70,71] have been correlated with PS rearrangement. Therefore, Annexin V may be used to indicate cell death based on the "classical analysis", but this view is no longer a definitive tool to declare apoptosis only.[66]

As indicated by our results, BT-474 and MDA-MB-231 cells treated at their respective IC_{50} values of the P3/SL-HE mixture (1:8 molar ratio), showed no significant Annexin V or SYTOX Red activity at 1, 3, and 6 h postdrug exposure (Figures 5A and S5A). However, at 9 h postdrug exposure, approximately 30% of BT-474 cells experienced early-stage apoptosis and 50% of cells experienced late-stage apoptosis (based on the "classical" view). For MDA-MB-231 cells, approximately 16 and 5% of cells experienced early-stage and late-stage apoptosis, respectively. Furthermore, the combined drug resulted in a significant increase in Annexin V binding activity compared with the untreated control. Statistical analysis by one-way ANOVA with the Tukey test showed significantly increased early apoptosis (p = 0.0002) and late apoptosis ($p < 0.0001$) against the untreated control for BT-474 cells, and ($p = 0.0115$) for early apoptosis in MDA-MB-231 cells compared to the untreated control (Figure S6). Representative flow cytometry data show a distinct shift in apoptotic pathways over time for BT-474 cells (Figure 5B−F) and MDA-MB-231 cells (Figure S5B−F). Additionally, cell death with PS rearrangement and lysis was analyzed for P3 singly and SL-HE singly (Figure S7) at the apparent IC_{50} of the combinations shown in Table 1. Significant cell death was not observed under these conditions.

A classical analysis of the Annexin V assay would indicate that apoptosis occurs for both cell lines; however, due to the challenges associated with PS translocation occurring in multiple programmed pathways, investigation of cell death was further analyzed by quantifying the key proteins APO-1/Fas for extrinsic apoptosis, Bcl-2 for intrinsic apoptosis, and LC3-II for autophagy.

https://doi.org/10.1021/acsomega.3c09902
ACS Omega 2024, 9, 33408−33424

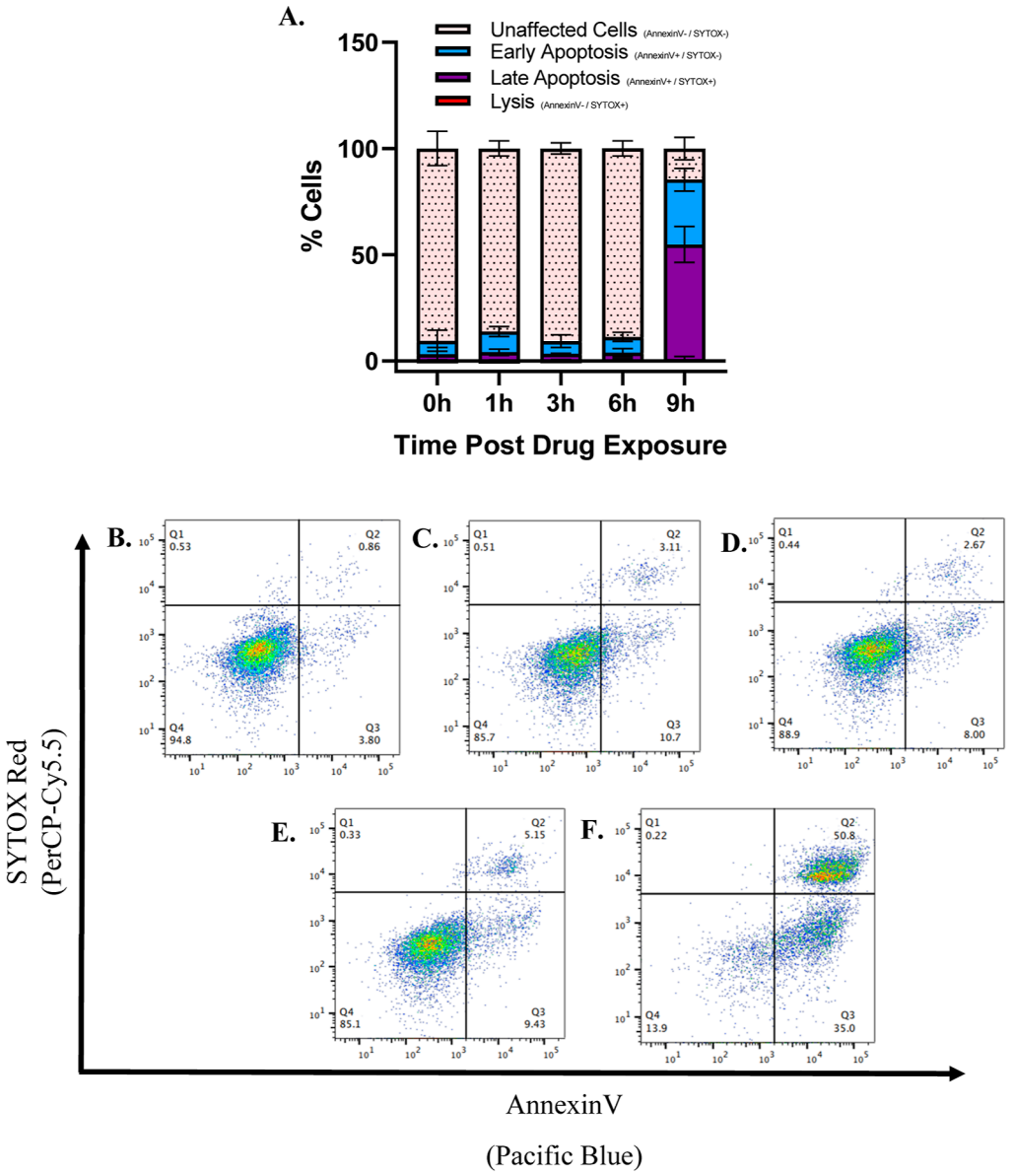

Figure 5. Analysis of BT-474 plasma membrane rearrangement induced by drugging with the 1:8P3/SL-HE combination at its IC_{50} concentration. Annexin V was used to label PS and SYTOX to bind DNA. The percentage of cells which were unaffected or show early apoptosis, late apoptosis, or cell lysis (A). Also displayed is a representative flow cytometric analysis at time points of 0 (B), 1 (C), 3 (D), 6 (E), and 9 h (F). One-way ANOVA with multiple comparison Tukey's test showed significant early ($p = 0.0002$) and late ($p < 0.0001$) apoptotic cells compared with untreated 0 h controls. n = 3/time point. Statistical analyses were performed using GraphPad Prism10.

Detection of Apo-1/Fas, LC3-II, and Bcl-2 in BT-474 and MDA-MB-231 Cells. To further investigate the mechanism of action leading from the translocation of PS to the outer leaflet of the cellular membrane, the expression of three proteins was quantified using ELISA. APO-1/Fas, also known as CD95, was selected as a reporter for extrinsic apoptosis.[51,72] The receptor Fas/APO-1 (CD95) is important in the regulation of immune development and termination of the immune response.[73] Fas is believed to be involved in tumor formation, progression, and immunity.[51,73−76] In BT-474 cells treated with the P3/SL-HE mixture, there was a slight increase in APO-1/Fas levels at 1 and 6 h postdrug exposure compared to the 0 h basal level control (Figure S8A). In the MDA-MB-231 cell line, there was no change in APO-1/Fas reported between hours 0 and 6 postdrug exposure. However, postdrug exposure, there was a slight decrease at 9 h. As reported by Hadji et al., downregulation of APO-1/Fas, correlates with necrotic cell death by mitotic catastrophe.[51] This type of cell death is characterized by a downregulation of APO-1/Fas, cell swelling, ROS production, DNA damage, and mitochondrial dysfunction.[51] Alternatively, the decrease may be due to a decrease in cell viability at 9 h postdrug exposure, thereby resulting in a decreased level of basal APO-1/Fas.

Since the primary mode of cell death was likely not regulated by an extrinsic mechanism, the Bcl-2 family was interrogated for intrinsic apoptosis (Figure S8B). As discussed above, the Bcl-2 family of proteins regulate and mediate the intrinsic pathway by which mitochondria cause cell death. Thus, mitochondrial dysfunction and the regulation of the Bcl-2 pro-apoptotic protein family are interconnected.[77] In particular, the downregulation of Bcl-2 can cause mitochondrial

https://doi.org/10.1021/acsomega.3c09902
ACS Omega 2024, 9, 33408−33424

fission, cytochrome *c* release, membrane depolarization, and mitochondrial pore formation.

LC3-II is a marker for autophagosomal membranes. This is due to that, during the fusion of lysosomes with intra-autophagosomes, lysosomal proteases degrade intra-autophagosomal LC3-II. The resulting changes in LC3-II cell concentrations are connected to the dynamic turnover of LC3-II via the autophagic activity by lysosomes.[78] The LC3-II ELISA indicated a slight increase in LC3-II at 9 h postdrug exposure in BT-474 cells (Figure S8C) and a steady decrease in MDA-MB-231 cells. An increase in LC3-II is related to the initiation of autophagy, whereas a decrease may be associated with a decline in viable cells (via a decline in basal levels).

When Bcl-2, an antiapoptosis (or pro-survival) protein, is downregulated, it is unable to bind to and inhibit the pro-apoptotic Bcl-2 members, Bax and Bak.[79−81] With the downregulation of Bcl-2, Bax and Bak are able to initiate the apoptotic caspase cascade and mitochondrial dysfunction.[81] In MDA-MB-231 cells treated with P3/SL-HE, a steady decline in Bcl-2 occurs from 0 to 9 h postdrug exposure (Figure S8B). The decrease in Bcl-2 paired with mitochondrial dysfunction and PS exposure on the outer leaflet of the membrane indicates that intrinsically mediated apoptosis occurs through mitochondrial dysfunction. In BT-474 cells treated with P3/SL-HE, a decrease in Bcl-2 from 1 to 6 h postdrug exposure indicates intrinsic apoptosis; however, at 9 h postdrug exposure, Bcl-2 is upregulated. The upregulation of Bcl-2 has been associated with the initiation of the NF-kβ inflammatory pathway, which in turn has been associated with the upregulation of autophagy.[81,82]

Cholesterol Extraction from Plasma Membrane. Cholesterol is located in the plasma membrane of mammalian cells and functions as an essential structural and functional component helping to stabilize cellular integrity while modulating signaling pathways.[83−85] Cholesterol typically congregates in lipid raft regions of the plasma membrane and promotes the regulation of cell proliferation, differentiation, and survival. In tumorigenic cells, cholesterol plays a role in angiogenesis, metastasis, and aggressiveness of certain tumors.[83−85] Cholesterol depletion from the plasma membrane has been associated with the induction of apoptosis, programmed necrosis, and autophagy, where the inactivation of the caspase cascade by lipid raft rearrangement has been related to induction of autophagy, necroptosis, paraptosis, and pyroptosis.[84] Additionally, disruption of lipid raft regions of tumorigenic cells is associated with increased sensitivity to chemotherapeutics.[84] Piscidin 1/3 (P1/3) is known to alter cholesterol distribution in membranes, causing lipid redistribution and restructuring of synthetic PC/cholesterol membranes.[13,17]

Seeking to mimic an assay by Wójtowicz et al.,[86] where the lipopeptide biosurfactant, surfactin, was shown to significantly reduce the cholesterol content in surviving CHO-K1 cells, both tumorigenic and nontumorigenic cells were dosed with the combined drug P3/SL-HE at respective IC_{50} values for 24 h while monitoring the cholesterol levels in the plasma membranes. Results indicate that P3/SL-HE caused significant disruption of the plasma membrane by means of cholesterol extraction in MDA-MB-231 ($p < 0.0001$) and BT-474 ($p = 0.0001$) cells, and a nearly significant extraction in CCD1065SK HDF cells ($p = 0.0527$) (Figure 6).

Interestingly, depletion of plasma membrane cholesterol has been associated with the impairment of the APO-1/Fas death signaling pathway, which was potentially upregulated at select time points for MDA-MB-231 and BT-474 cells (Figure S8A).[87] Thus, these results are consistent. Additional information on the extraction of cholesterol from the plasma membrane from P3 singly and SL-HE singly on all cell lines can be seen in Figure S9, where cholesterol was depleted from P3 singly and SL-HE singly for both tumorigenic cells lines but not for nontumorigenic HDF cells. Further biophysical studies are necessary to determine how the combined drug interacts with plasma membranes and how the relative fatty acid and cholesterol compositions affect the disruption of membrane organization. These results indicate that the combined drugs interact with the plasma membrane of tumorigenic cells, sensitizing them to enhanced cell death by intrinsic apoptosis or programmed necrosis.

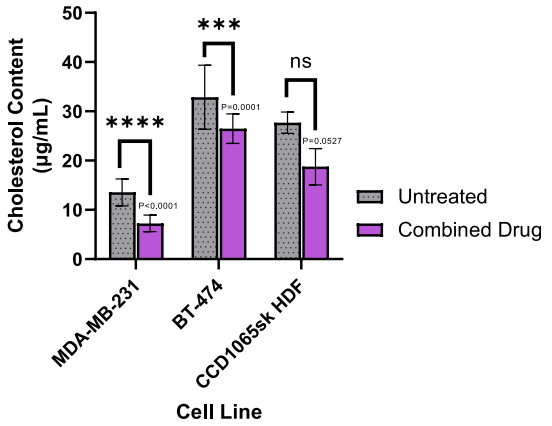

Figure 6. Analysis of cholesterol extracted from the plasma membrane of MDA-MB-231, BT-474, and CCD1065SK HDF breast cells after a 24 h exposure to the combined drug at its respective IC_{50} values. Significance was determined using a Student's *t*-test using $n = 9$/sample for tumorigenic and n = 3/sample for nontumorigenic cell lines.

Scanning Electron Microscopy. Electron microscopy is an indispensable tool for the identification of physical modifications to tumorigenic cells after their exposure to different chemotherapeutics. Cell preservation techniques were used to visualize whether dosing of BT-474 and MDA-MB-231 with the combination drug for 24 h at the respective IC_{50} values induced morphological features characteristic of apoptosis, necrosis, programmed necrosis, and/or autophagy. Apoptosis is distinguished by cells with decreased size, loss of contact points (microvilli and cell−cell junctions), a cup-shaped nuclear envelope, progressive fragmentation, and apoptotic body formation.[70,88] Evidence of apoptosis is apparent in both BT-474 (Figure 7) and MDA-MB-231 (Figure 8) tumorigenic cells exposed to P3/SL-HE where white arrows in Figures 7C,D and 8C,D point to cell shrinkage, decrease in cell attachment, and the formation of apoptotic bodies. While there is no evidence of primary necrosis, there are signs of programmed necrotic pathways, pyroptosis and necroptosis (red and black arrows in Figures 7 and 8). Pyroptosis is characterized by cells which have gradual flattening, membrane pore formation, and pyroptotic bodies.[70,88,89] Similarly, necroptosis is characterized by necroptotic body formation, ruptured membranes, and general cell swelling.[70,88] BT-474 (Figure 7C,D) and MDA-MB-231 (Figure 8E,F) cells showed evidence of programmed necrosis by black and red arrows, indicating swollen or flattened cells,

https://doi.org/10.1021/acsomega.3c09902
ACS Omega 2024, 9, 33408−33424

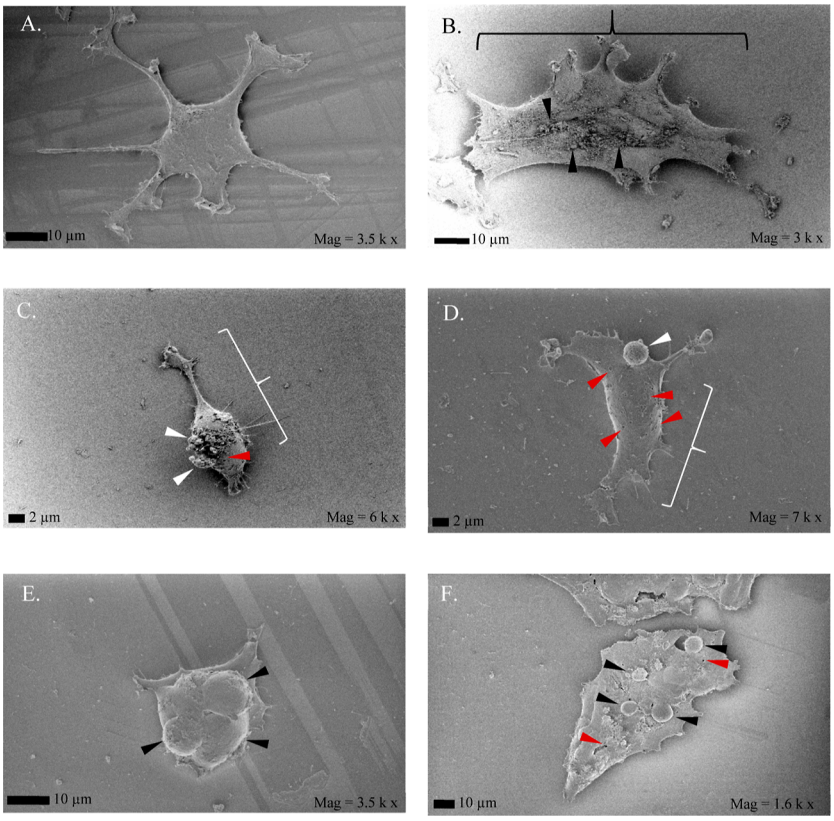

Figure 7. Scanning electron microscopy of BT-474 cells after combined drug exposure. SEM images of BT-474 untreated (A), dosed for 24 h at the IC_{50} (B,C), and 2 × IC_{50} (D−F). White arrows point to areas consistent with apoptotic cell death, including cell shrinkage and plasma membrane blebbing. Black arrows point to areas consistent with programmed necrosis, including cell flattening or swelling, pore formation (red arrows), and pyroptotic/necroptotic bodies.

pore formation, and pyroptotic/necroptotic bodies. Results indicate that multiple modes of cell death are visually apparent after exposure to the IC_{50} or 2 × IC_{50} for 24 h. Morphological characteristics, visualized by SEM, align with our assessment that intrinsic apoptosis occurs in both cell lines, as determined by white arrows, and provide evidence that secondary pathways from extended exposure to the combined drugs can be activated (black and red arrows).

DISCUSSION

The synergy between multiple cosecreted compounds is often found in nature to provide protection against pathogenic interference.[1,6] In this study, we sought to understand the synergism between two antimicrobial compounds, P3 and SL-HE, and their effect against breast cancer cells. Synergy is often evaluated using "checkerboard" experiments, where a two-dimensional array of serial dilutions is used to determine the FIC value.[7] As indicated by eq 1, FIC is determined as the sum of the ratio of each component singly divided by each component in combination. FIC < 1 is synergistic, whereas FIC > 1 is antagonistic.[7] Previous work by our group evaluated the effects of two piscidins (P1/3) and two SLs (SL-HE and SL-butyl ester). Synergy was observed against *B. cereus* for concentrations of 1 μM P3 and 8 μM SL-HE with FIC = 0.25.[42] Permeabilization assays and biophysical studies demonstrated a novel mechanism of action where the SL-HE micelles prefold the peptide and help deliver it to pathogenic membranes. Importantly, combining P3 with SL-HE resulted in synergistic accumulation of the agents within phospholipid bilayers as well as increased bilayer disruption.[42] These studies motivated the current research where the biological activities of singly administered agents P3 and SL-HE and their combination in a 1:8 molar ratio were investigated against two tumorigenic breast cell lines, MDA-MB-231 and BT-474, and the nontumorigenic CCD1065SK HDF cells.

Dose−response curves and the subsequent apparent IC_{50} values indicated that BT-474 cells were more sensitive to inhibition by the combined drug compared to the MDA-MB-231 cells. This is expected, as the BT-474 cells are typically regarded as easier to treat, less aggressive, and less metastatic than the MDA-MB-231 cells.[60,90] With FIC values <1, the combined drugs are shown to induce a synergistic effect on both MDA-MB-231 and BT-474 cells, with an effect greater for BT-474 than MDA-MB-231 cells. Nontumorigenic CCD1065SK HDF cells, which experienced high toxicity from SL-HE singly, revealed an increased IC_{50} value and thus lower toxicity when dosed with the P3/SL-HE combination. Thus, the addition of P3 to SL-HE exhibited a strong protection of normal cells, enabling an improved survival of these cells at higher concentrations of the combined drug.

For CCD1065SK HDF cells, the FIC value is 22 (Table 1), revealing a high extent of antagonism. Based on previous studies using circular dichroism experiments, we hypothesized that P3 can bury hydrophobic side chains in the nonpolar region of SL-HE micelles where the acyl tails of the glycolipid reside.[42] Furthermore, cationic P3 has a higher affinity for biological membranes than the SL-HE singly.[42] Since the outer leaflet of tumorigenic cells have more anionic PS than normal cells, these have phospholipid content that is close to net

https://doi.org/10.1021/acsomega.3c09902
ACS Omega 2024, 9, 33408−33424

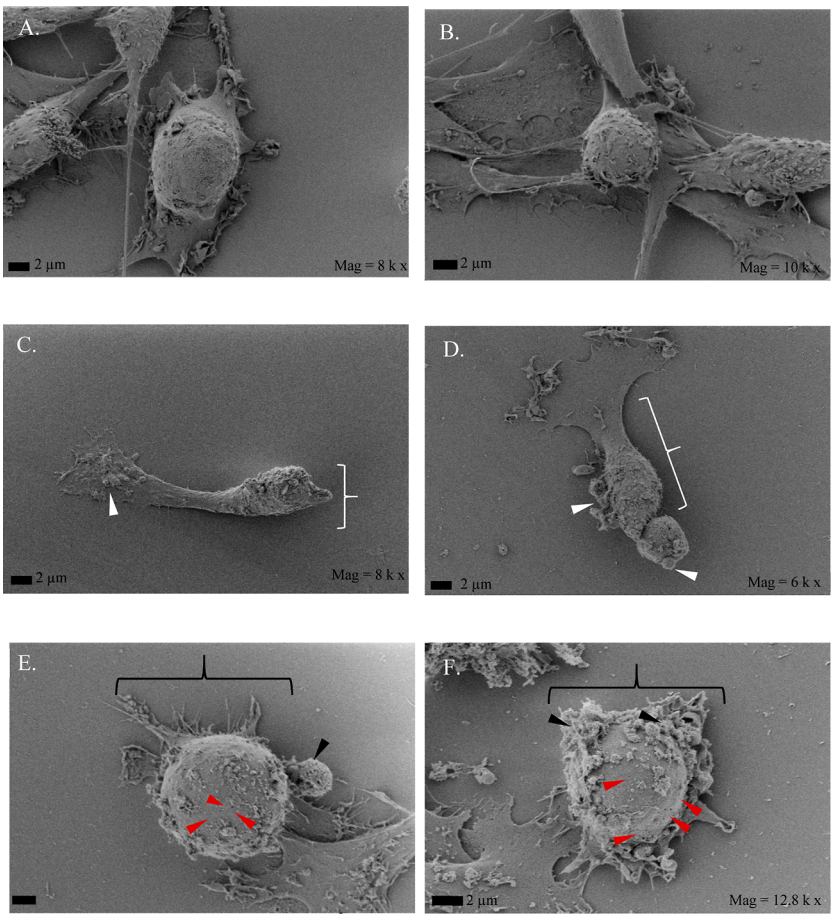

Figure 8. Scanning electron microscopy of MDA-MB-231 cells after combined drug exposure. SEM images of MDA-MB-231 cells untreated (A,B), dosed for 24 h at IC_{50} (C) and 2 × IC_{50} (D−F). White arrows point to areas consistent with apoptotic cell death, including cell shrinkage and plasma membrane blebbing. Black arrows point to areas consistent with programmed necrosis, including cell flattening or swelling, pore formation (red arrows), and pyroptotic/necroptotic bodies.

neutral or slightly cationic.[91] The complexed drugs could be repelled by the nontumorigenic plasma membrane. This would explain how P3 acts as an antagonist protector for nontumorigenic cells.

A SI > 3 is generally considered acceptable for continued studies with possible chemotherapeutics.[49] The SI of IC_{50} values obtained for the combined drugs were greater than 3, with the SI for BT-474 cells being 2.8-fold greater than that for MDA-MB-231 cells. Overall, the SI values indicate that the combination drug P3/SL-HE has improved selectivity compared to SL-HE used singly (where SI ∼ 0.1 for both cell lines). This suggests that P3 may protect nontumorigenic cells from the mechanistically driven cell death pathway that occurs at low drug concentrations in the tumorigenic cells. As mentioned above, this may be due to the phospholipid composition varying in different cell lines. Additional biophysical investigations are necessary to elucidate the apparent protection of nontumorigenic cells from high SL-HE toxicity.

While both tumorigenic cells dosed with P3/SL-HE responded similarly, there were notable differences in results. During the first 9 h of exposure, MDA-MB-231 cells expressed a significant increase in mitochondrial superoxide, whereas BT-474 cells did not. Both tumorigenic cell lines exhibited significant increases in ROS of 24 h. This may be due to differences in metabolic activity of the BT-474 cells compared with MDA-MB-231 cells, or due to a time course that was not conducive to capturing rapid changes in mitochondrially generated ROS.[90] Additional time points prior to 1 h and beyond 9 h may be necessary to fully capitulate the effects of the combined drug on BT-474 cells. In a short-course drug study, both cell lines expressed a dramatic decrease in cellular ATP levels; however, only the BT-474 cell line expressed an increase in cell lysis at higher combined drug concentrations. This may reflect an increased susceptibility for lysis or pore formation of the plasma membrane in BT-474 cells when exposed to the combined drug. Interestingly, BT-474 and MDA-MB-231 cells have vastly differing plasma membrane compositions, where the plasma membrane of BT-474 cells possess increased long-chain fatty acids and significantly differing PC and cholesterol levels compared to MDA-MB-231 cells.[61] Indeed, highly motile cells, such as the MDA-MB-231 cell line, are characterized by low cholesterol levels and high levels of unsaturated lipids, whereas nonmotile cells, such as BT-474 cells, possess high levels of cholesterol.[92] Results from the cholesterol extraction assay indicate that significant plasma cholesterol was extracted from both cell lines, although a higher concentration of cholesterol was detected in BT-474 cells. Also, both MDA-MB-231 and BT-474 cell lines exhibited significant increases of PS rearrangement from the inner to the outer leaflet of the plasma membrane from 9 to 24 h drug exposure time periods. However, more significant PS

https://doi.org/10.1021/acsomega.3c09902
ACS Omega 2024, 9, 33408−33424

rearrangement was recorded for BT-474 cells compared to the MDA-MB-231 cells. This may be due to variations in the levels of PS found in MDA-MB-231 vs BT-474 cells.[93] Further investigations are needed to understand how the metabolic rates and plasma membrane compositions can play a role in the biological activities of the combined drug against tumorigenic cells.

Previous work indicated that tilapia piscidin 3 (TP3) induces a mitochondrial-modulated intrinsic apoptotic mechanism against osteosarcoma and inhibited its motility by modulation of the tumor microenvironment of glioblastoma cells.[9,18] Against triple-negative breast cancer, tilapia piscidin 4 (TP4) induced a selective necrotic mechanism of action and mitochondrial dysfunction through the FOSB pathway.[11] Natural DLSL was said to induce apoptosis on MDA-MB-231 and ovarian (HeLa) cells.[34,94] However, in-depth studies revealing mechanism(s) of cell death on tumorigenic cells as induced by modified SL esters are lacking beyond the elucidation of significantly increased M2 phenotyping of macrophages upon exposure to modified SL esters.[34,38,95] The proposed mechanisms of action of the combination drug presented herein are consistent with previously published mechanism(s) of action of piscidins against tumorigenic cells, which include the evidence of necrosis, apoptosis, and ROS formation.[11,12,18,96,97] However, our results obtained here show that multiple actions are induced from exposing the MDA-MB-231 and BT-474 cells to the combined drug P3/SL-HE. For example, BT-474 cells exhibited downregulation of Bcl-2 when exposed to the combined drug for 1−6 h. This is consistent with intrinsic apoptosis. However, the upregulation of both Bcl-2 and LC3-II was observed at 9 h is associated with autophagy. Thus, multiple modes of time-dependent cell death are detected. This introduced the possibility of programmed apoptosis as a primary mode of cell death, followed by a secondary programmed autophagy.[98−100] In the case of MDA-MB-231 cells, we observed a downregulation of APO-1/Fas after 9 h of exposure to P3/SL-HE. This points to the necrotic mechanism of cell death by mitotic catastrophe.[51,101] Finally, MDA-MB-231 and BT-474 cells imaged by SEM exhibited morphological features consistent with apoptosis (cell shrinkage, blebs, and apoptotic bodies) as well as programmed necrosis (pore formation, general flattening or ballooning of cells, blebs, and body formation). Hence, multiple forms of cell death can occur from the introduction of drugs singly or in combination due to the interconnectedness of protein signaling pathways responsible for apoptosis, autophagy, and programmed necrosis.[101−105] Further investigations that explain the biological activities on tumorigenic cell lines of P3/SL-HE and expand these studies to a broader range of modified SLs and antimicrobial peptides will provide valuable information on strategies to increase antitumor efficacy and selectivity, the latter being critical to reduce detrimental side effects.

The graphical abstract summarizes the physiological and biochemical effects of dosing MDA-MB-231 and BT-474 tumorigenic cells with the combined drug P3/SL-HE in a 1:8 mol/mol ratio at its IC_{50}. The combined drug induced an intrinsically mediated mechanism of cell death via the induction of ROS and mitochondrial dysfunction, leading to a proposed Bcl-2-regulated intrinsic apoptosis and a secondary programmed necrotic or autophagic pathway (graphical abstract). The Bcl-2 family of proteins are important regulators of intrinsic apoptosis. They downregulate "pro-survival" Bcl-2 and upregulate pro-apoptotic proteins Bax and Bak, which initiate mitochondrial dysfunction through pore formation in the mitochondrial membrane.[79] Growth factor depletion or intracellular stress can induce intrinsic apoptosis, whereas extrinsic apoptosis is initiated through transmembrane receptors.[51,52,79,106] Results from Bcl-2 and APO-1/Fas ELISA indicate that the combination drug induced the down-regulation of Bcl-2 and only slight changes to APO-1/Fas, a protein upregulated in extrinsic apoptosis.[51,52,99,106]

CONCLUSIONS

In conclusion, this work showed that P3 and SL-HE in a 1:8 molar combination provides a novel synergistic effect against two vastly different tumorigenic breast cells, MDA-MB-231 and BT-474 cell lines. BT-474 cells, generally regarded as an easier-to-treat cell line, had increased activity and selectivity over the harder-to-treat MDA-MB-231 cells. Synergistic effects were confirmed through promising dose−response curves, IC_{50} values, synergistic FIC values, and subsequent biological activities of the novel 1:8 molar combination of P3/SL-HE. Comparing the results of the combination drug with those of each drug singly indicated improved cytotoxicity and SI values. Additionally, dosing BT-474 and MDA-MB-231 cells with the combination drug at corresponding IC_{50} values caused an intrinsically mediated mechanism of action through both apoptosis and programmed necrosis, regulated by increased ROS, mitochondrial dysfunction, plasma membrane disruptions, and a downregulation of Bcl-2, for both tumorigenic cell lines.

Limitations and recommendations for future studies include a checkerboard protocol for investigating the improved synergy from varied molar ratios of P3 and SL-HE, as well as an investigation of P1—which has improved membrane permeabilizing potential, or including a known chemotherapeutic such as doxorubicin.[12,13,17] Our biophysical understanding of the interactions of P3 and SL-HE occurred at pH 7.4.[42] However, the pH of tumorigenic extracellular environments is slightly lower, pH ∼ 6.7−7.1.[107] Future studies, including cytotoxicity, size, zeta potential, micelle stability, long-term cell line exposure, and electron microscopy, of the P3/SL-HE complex in tumor acidic pH conditions are necessary to understand the biophysical interactions in a physiologically relevant environment. Additionally, future tests including an increased number of dilutions on a wide variety of tumorigenic or non-tumorigenic cell lines would strengthen the synergistic understanding of the cytotoxicity of the combined drug. Lastly, RNA sequencing transcriptomic and metabolomic data sets, as well as the use of free, open-access programs such as Combenefit, should be utilized to investigate multiple mechanisms of action, cytokine/chemokine regulation, and caspase activation from the exposure of tumorigenic cells to the combined drug.

To our knowledge, this is the first study to investigate the synergistic effects of P3 and SL-HE on tumorigenic cells in a 1:8 molar ratio, and the first to propose multiple mechanisms of action; apoptosis and programmed necrosis. The synergistic anticancer effects combined with the protective properties on normal cells are particularly notable in the search for novel drugs to fight cancer.

https://doi.org/10.1021/acsomega.3c09902
ACS Omega 2024, 9, 33408−33424

MATERIALS AND METHODS

Materials, Peptide Synthesis, and Purification. The piscidin peptide P3 (FIHHIFRGIVHAGRSIGRFLTG; MW: 2492) was synthesized with carboxyamidated ends by solid-phase peptide synthesis at the University of Texas Southern Medical Center, and the resulting P3 was purified and assessed for purity by HPLC and mass spectroscopy according to previously published protocols.[14,108,109] Peptide stock concentrations of approximately 330 μM were reconstituted in nanopure water, and stock concentrations were determined by amino acid analysis performed at the Protein Chemistry Center Texas A&M (College Station, TX). SL-HE was synthesized according to previously published protocols from the natural DLSL produced from the fermentation of *S. bombicola*; structural characterization and purity confirmation were done by NMR and mass spectroscopy.[29−31,38]

Cell Culture Materials. CCD-1065SK HDFs (ATCC, Manassas, VA), derived from the mammary epithelial tissue, were grown in standard cell culture conditions (37 °C, 5% CO_2, and 95% RH) in Dulbecco's modified Eagle medium (DMEM) without phenol red, supplemented with 15% (v/v) fetal bovine serum (FBS) and 0.5% (v/v) penicillin/streptomycin. MDA-MB-231 triple-negative human breast adenocarcinoma cells and BT-474 human breast ductal carcinoma cells (ATCC, Manassas, VA) were grown in standard cell culture conditions (37 °C, 5% CO_2, and 95% RH) in DMEM without phenol red, supplemented with 10% (v/v) FBS and 0.5% (v/v) penicillin/streptomycin.

2D Dose−Response Assay. To prepare 2D monolayer cultures, cells were trypsinized, centrifuged, and resuspended in media at 250,000 cells/mL. A 100 μL cell suspension was added to each well of a 96-well plate flat bottom, and cells were cultured for 24 h prior to compound testing. Compounds were individually prepared; SL-HE was initially solubilized in 100% DMSO and serially diluted 1:1 in cell media. P3 stock solution (in H_2O) was serially diluted 1:1 in cell media, and the combined drug was prepared by mixing 8 parts of SL-HE and 1 part of P3. The initial concentration of P3 in combination was 33 μM, and the initial concentration of SL-HE in combination was 264 μM. The SL-HE singly was initially dosed at 707 μM, and the P3 singly was initially dosed at 66 μM. All samples were subjected to a 1:1 dilution with cell culture media, resulting in a 50% reduction in potency for each subsequent dilution (e.g., 707 μM, 353.60 μM, 176.8 μM, etc.). The drug combination mixture was maintained at RT for 30 min prior to 1:1 serial dilution using cell media. The highest final concentration of DMSO was 0.22%, and following serial dilutions the lowest DMSO concentration was 0.002%. Thus, we assume the cytotoxicity from DMSO was negligible, as this is a standard approach to drug solubilization and cell dosing. Negative and positive controls consisted of wells containing only media and untreated cells, respectively. After drug addition, cells were placed in a standard cell culture incubator (5% CO_2, 37 °C) for 24 h, and cell viability was assessed by the Cell Counting Kit-8 (CCK-8) assay, following the manufacturer's protocol,[45] and using a BioTek μQuant Microplate Reader (BioTek Instruments). The half-maximal inhibitory concentration (IC_{50}) was calculated with the use of GraphPad Prism10 software. Absolute IC_{50} determination: In Table 1, we have calculated the IC_{50} of each drug individually within the 1:8 molar ratio and reported this as the apparent IC_{50}. In these calculations, we assume that a 1:8 molar ratio is consistent throughout the dilution process. The apparent IC_{50} values shown were calculated through a technical replicate of three, as is a standard practice for these calculations.

The respective IC_{50} concentrations were utilized to determine the FIC using the equation shown below

$$\mathrm{FIC} = \left(\frac{C[\mathrm{P3}]}{\mathrm{IC}_{50}[\mathrm{P3}]}\right) + \left(\frac{C[\mathrm{SL\text{-}HE}]}{\mathrm{IC}_{50}[\mathrm{SL\text{-}HE}]}\right) \quad (1)$$

where C[P3] and C[SL-HE] are, respectively, IC_{50} values of P3 and SL-HE when they are acting alone, and IC_{50}[P3] and IC_{50}[SL-HE] are the corresponding IC_{50} values of each drug in combination. FIC < 1 indicates the synergy between compounds, and FIC > 1 indicates antagonism.[7]

Selectivity Index. The selectivity index (SI) is a measurement of the safety window between cytotoxicity and anticancer activity of the drugs singly or in combination. The following equation was used to evaluate the effectiveness of P3, SL-HE, and their combination, where "IC_{50} nontumorigenic cells" is the IC_{50} (or FIC) against the CCD1065SK HDF cell line, and "IC_{50} tumorigenic cells" is the IC_{50} (or FIC) against either MDA-MB-231 or BT-474 cells.

$$\mathrm{SI} = \frac{\mathrm{IC}_{50}\ \text{nontumorigenic cells}}{\mathrm{IC}_{50}\ \text{tumorigenic cells}} \quad (2)$$

Mitochondrial Dysfunction Assay. Following the manufacturer's protocol,[110] the Mitochondrial ToxGlo assay was used to determine the mitochondrial dysfunction after a 90 min exposure to the drug combination. Briefly, MDA-MB-231 or BT-474 cells were seeded at 100,000 cells/mL in a 96-well plate (100 μL of cell suspension per well). After allowing cell attachment, cells were dosed at their respective IC_{50} values and incubated for 90 min. Following incubation, the ATP detection reagent was added to each well and briefly mixed by orbital shaking. The experimental samples and ATP detection reagent were placed in a 37 °C incubator for 30 min. Fluorescence was recorded at 485 nm excitation and 520 nm emission. The plate was then equilibrated to RT for 10 min, and 100 μL of ATP detection reagent was added to each well. The assay was left at RT for an additional 10 min after shaking. The luminescence was recorded under scanning luminescence mode. The data were normalized to the vehicle control and plotted using GraphPad Prism10. Data were recorded using the Tecan Infinite M1000 PRO Multi-Well Plate Reader.

CellROX Assay for Oxidative Stress Detection Using Flow Cytometry. Following manufacturer's protocol,[111] CellROX reagent was used to determine ROS from compound exposure. Briefly, MDA-MB-231 or BT-474 cells were seeded at 200,000 cells/mL in a 96-well plate (100 μL of cell suspension per well). After allowing cell attachment, cells were dosed at their respective IC_{50} values and incubated for 24 h. The following day, the CellROX reagent was added directly to the medium in each well at a final concentration of 5 μM, and cells were again incubated at 37 °C with 5% CO_2 and 95% RH for 30 min. After incubation, the medium was aspirated, and the cells were washed with PBS once, trypsinized, and centrifuged. Cell pellets were washed in PBS once more and resuspended in 100 μL of PBS. The cell suspension was exposed to 1 μg/mL propidium iodide to detect cell lysis and allowed to incubate at RT for 15 min with a lack of light exposure. Cells were resuspended in FACS tubes at 500 μL and placed on ice until analysis. Data collection was completed

https://doi.org/10.1021/acsomega.3c09902
ACS Omega 2024, 9, 33408−33424

using an LSR II flow cytometer, and data analysis was completed using FlowJo, version 10.8.

Annexin V/AADvanced SYTOX Red Flow Cytometry Assay. Following the manufacturer's protocol,[112] Annexin V reagent (Thermo Fisher #A35122) was used to determine apoptosis via phospholipid phosphatidylserine (PS) exposure from drug exposure. Additionally, SYTOX Red (Thermo Fisher #S34859) was used to determine cell death from lysis. MDA-MB-231 or BT-474 cells were seeded at 200,000 cells/mL in a 96-well plate (100 μL of cell suspension per well). After allowing cell attachment, cells were dosed at their respective IC_{50} values and incubated for 1, 3, 6, 9, and 24 h. After incubation, cells were harvested and washed in cold PBS twice, and resuspended in 100 μL of Annexin V binding buffer. Then, 5 μL of Annexin V and 1 μL of SYTOX Red was added to each sample. Samples were left to incubate in the dark for 15 min at RT. Cells were further diluted in an additional 400 μL of binding buffer, transferred to FACS tubes, and placed on ice until analysis. Data collection was completed using an LSR II flow cytometer, and data analysis was completed using FlowJo, version 10.8.

Mitochondrial Superoxide Assay. Invitrogen MitoSOX Red mitochondrial superoxide indicator (Thermo Fisher Cat#M36005)[113] was used to determine mitochondrial superoxide formation from drug exposure in MDA-MB-231 or BT-474 cells. Briefly, cells were seeded at 200,000 cells/mL in a 96-well tissue culture plate. After allowing for proper cell attachment, cells were incubated in the absence or presence of their respective IC_{50} values for the 1:8 combination drug for 1, 3, 6, and 9 h. Following incubation, the supernatant was removed from each well, cells were trypsinized, washed once in warm media, and resuspended in 50 nM MitoSOX MSR reagent. Cells were returned to 37 °C and 5% CO_2 for 30 min. After incubation, cells were washed once with warm PBS and resuspended in 300 μL PBS. Samples were placed on ice, and data collection was completed using a LSR II flow cytometer, and data analysis was completed using FlowJo, version 10.8.

Human sAPO-1/Fas ELISA. An Invitrogen Human sAPO-1/Fas ELISA kit (Thermo Fisher cat# BMS245) was used according to manufacturer's protocol[114] to determine the expression of APO-1/Fas protein in its initiation of extrinsic apoptosis. Briefly, the supernatant from the mitochondrial superoxide assay, which was previously pooled and frozen, was thawed at RT for 30 min. Each microwell of the ELISA plate was washed twice with wash buffer, and 100 μL of sample diluent and a 1:2 dilution of APO-1/Fas stock was added to each well to create the APO-1/Fas standard curve. Next, 90 μL of sample diluent was added to each experimental well, and 100 μL of sample diluent was added to blank wells. Each experimental sample was run in duplicate by adding 10 μL of cell supernatant to each corresponding well. Next, 50 μL of biotin conjugate was added to all wells, and the plate was left to incubate at 37 °C for 1 h. After incubation, the plate was washed twice with wash buffer, and 100 μL of 0.5 μg/mL Streptavidin−HRP was added to all wells. The plate was incubated for 1 h at 37 °C. After incubation, the plate was washed with wash buffer, and 100 μL of tetramethylbenzidine (TMB) substrate solution was added to each well. The plate was incubated at RT until a visible color change was observed or for about 10 min. Next, 100 μL of 1 M phosphoric acid Stop solution was added to each well. Data were recorded by reading the absorption at 450 nm using a Tecan Infinite M1000 PRO Multi-Well Plate Reader.

Human Bcl-2 ELISA. An Invitrogen Human Bcl-2 ELISA kit (Thermo Fisher cat# BMS244-3) was used according to manufacturer's protocol to determine the expression of Bcl-2 protein in its initiation of intrinsic apoptosis. Briefly, the supernatant from the mitochondrial superoxide assay, which was previously pooled and placed at −20 °C was thawed at RT for 30 min. Each microwell of the ELISA plate was washed twice with 400 mL wash buffer, and 100 μL of 1:2 dilution of Bcl-2 stock was added to each well to create the standard curve. Next, 80 μL of sample diluent was added to each experimental well, and 100 μL of sample diluent was added to blank wells. Each experimental sample was run in duplicate by adding 20 μL of cell supernatant to each corresponding well. Next, 50 μL of biotin conjugate was added to all wells, and the plate was left to incubate at RT for 2 h on a plate shaker. After incubation, the plate was washed twice with wash buffer, and 100 μL of Streptavidin−HRP was added to all wells. The plate was incubated for 1 h at RT on a plate shaker. After incubation, the plate was washed with wash buffer, and 100 μL of TMB substrate solution was added to each well. The plate was incubated at RT until a visible color change was recorded, or for about 10 min. Next, 100 μL of Stop solution was added to each well. Data were recorded by recording the absorption at 450 nm using a Tecan Infinite M1000 PRO Multi-Well Plate Reader.

Human LC3-II ELISA. A Cell BioLabs Autophagy ELISA kit (LC3-II Quantitation) (Cat# CBA-5116) was used according to manufacturer's protocol[115] to determine the expression of LC3-II protein in its initiation of autophagy. Briefly, MDA-MB-231 or BT-474 cells were trypsinized and resuspended in 500,000 cells/mL and seeded into a 6-well tissue culture plate and allowed to adhere overnight in a tissue culture incubator. The following day, old media was discarded, and 1800 μL of warm tissue culture media was added to each well, as well as 200 μL of the combined drug was added to the corresponding cell line on a time course schedule. After proper incubation (9, 6, 3, or 0 h), the supernatant was discarded, and cells were carefully washed 3× with 1× PBS containing 1 mM $MgCl_2$ and 1 mM $CaCl_2$. Cells were then incubated at RT for 5 min with shaking, with the addition of 1 mL of 1× Cytosolic LC3 Removal Reagent. Cells were then carefully washed 3× with 1× PBS containing 1 mM $MgCl_2$ and 1 mM $CaCl_2$. 200 μL of ice-cold 1× RIPA buffer was added per well, and plates were incubated on ice for 10 min to allow for cell lysis. Cells were detached from the plate by cell scraping, and lysates were transferred to tubes and centrifuged for 10 min at 4 °C at 12,000*g*. The resulting supernatants were collected and stored at −80 °C for the following day. Utilizing the provided ELISA 96-well plate, 100 μL of lysate sample was added to each corresponding well, and LC3 standard was prepped. The plate was allowed to incubate for 2 h at 37 °C. Following incubation, the plate was washed 3× with wash buffer, and 100 μL of diluted anti-LC3 antibody was added to each well and allowed to incubate at RT for 2 h on an orbital shaker. Following incubation, the plate was washed 3× with wash buffer, and 100 μL of HRP-conjugated antibody was added to each well. The plate was allowed to incubate at RT for 1 h on an orbital shaker. Following incubation, the plate was washed 3× with wash buffer, and 100 μL of substrate solution was added to each well. The plate was allowed to incubate at RT on an orbital shaker until color change was observed, and then 100 μL of Stop solution was added to each well. Data were

https://doi.org/10.1021/acsomega.3c09902
ACS Omega 2024, 9, 33408−33424

recorded immediately by recording the absorption at 450 nm using a Tecan Infinite M1000 PRO Multi-Well Plate Reader.

Membrane Cholesterol Extraction Assay. Following a protocol by Wójtowicz et al.,[86] the cholesterol content from plasma membrane extraction was completed. In brief, MDA-MB-231, BT-474, or CCD1065SK HDF cells were seeded at 200,000 cells/mL in a 24-well tissue culture plate. After 24 h of drug exposure at respective IC_{50} values, cell media was aspirated, trypsinized, and cells were washed three times with PBS buffer and lysed with RIPA buffer for 30 min on ice. Lysates were then centrifuged at 10,000*g* for 10 min at 4 °C, and the supernatant was transferred to a fresh 1 mL tube. Total cholesterol level was determined following manufacturer's protocol for the Ample Red Cholesterol Assay Kit.[116] Briefly, 50 μL of cell lysate was mixed with 50 μL of Amplex Red reagent working solution and incubated for 30 min at 37 °C without light present. Fluorescence was measured using a μQuant Microplate Reader (BioTek Instruments) at 520 nm excitation and 560 nm emission. The background was subtracted from the final value, and all wells were normalized to the total amount of protein in each sample, as quantified by the Bradford protein assay. The total cholesterol content for each sample was calculated in μg/mL, as determined by a standard curve. Data were recorded by recording the absorption at 450 nm using a Tecan Infinite M1000 PRO Multi-Well Plate Reader.

Scanning Electron Microscopy. MDA-MB-231 and BT-474 cells were trypsinized and resuspended at 100,000 cells/mL. In a 12-well tissue culture-treated plate, 1 mL of warm media and 1 mL of cell suspension were added to each well of the plate, where a tissue-culture treated coverslip was added to the bottom of each well. Three wells of MDA-MB-231 and three separate wells of BT-474 cells were left to attach overnight in a tissue culture incubator (37 °C and 5% CO_2). After attachment, old media was discarded, and 1000 μL of fresh media was added to each well. Next, 100 μL of the combined drug was added to each respective well at their IC_{50} and 2× IC_{50} for a 24 h incubation (i.e., 16 and 8 μM of P3 for MDA-MB-231 and 8 and 4 μM of P3 for BT-474, in 1:8 synergy with SL-HE). After incubation at 37 °C and 5% CO_2 for 24 h, the supernatant was removed, and cells were fixed in a 2.5% solution of glutaraldehyde for 30 min. Cells were then washed with an ethanol gradient (10, 30, 40, 60, 80, 90, and 100% ethanol) for 15 min at each concentration. Coverslips were freeze-dried using a Tousimis Critical Point Dryer in 100% ethanol. Each slide was attached to a coverslip clamp apparatus with double-sided carbon tape, with one point connected to the apparatus via silver paint. The samples were sputter-coated with platinum for 60 s at 30% to decrease the charging of the material. Cells were then imaged with a Supra 55 SEM at 0.5−2.5 kV.

Statistical Analysis. One-way ANOVA with either Tukey's or Fisher's LSD test for multiple comparisons, or unpaired Student's *t* tests were used for experimental analysis as indicated. Data are presented as mean with SD as indicated. Replicates were used as indicated. Data were analyzed and visualized using GraphPad Prism10. Symbol meanings: ns $p > 0.05$, $*p \leq 0.05$, $**p \leq 0.01$, $***p \leq 0.001$, and $****p \leq 0.0001$.

■ ASSOCIATED CONTENT

Supporting Information

The Supporting Information is available free of charge at https://pubs.acs.org/doi/10.1021/acsomega.3c09902.

Dose−response curves; flow cytometry gating; total intracellular ROS levels; total mitochondrial superoxide levels; analysis of MDA-MB-231 plasma membrane rearrangement; statistical analysis of plasma membrane rearrangement of MDA-MB-231 and BT-474 cells; analysis of MDA-MB-231 and BT-474 cells' plasma membrane rearrangement after single-drug dosing; detection of Apo-1/Fas, LC3-II, and Bcl-2 in MDA-MB-231 and BT-474 cells; and total extracted cholesterol from plasma membranes of MDA-MB-231, BT-474, and CCD1065SK HDF cells (PDF)

■ AUTHOR INFORMATION

Corresponding Authors

Myriam Cotten − *Department of Applied Science, William & Mary, Williamsburg, Virginia 23185, United States;* orcid.org/0000-0002-6732-1736; Email: mcotten@wm.edu; Fax: (757)-221-2050

Richard A. Gross − *Department of Chemistry and Chemical Biology, Rensselaer Polytechnic Institute, Troy, New York 12180, United States; Center for Biotechnology and Interdisciplinary Sciences, Rensselaer Polytechnic Institute, Troy, New York 12180, United States;* orcid.org/0000-0002-5050-3162; Email: grossr@rpi.edu; Fax: (518)-276-3405

Authors

Rebecca T. Miceli − *Department of Chemistry and Chemical Biology, Rensselaer Polytechnic Institute, Troy, New York 12180, United States; Center for Biotechnology and Interdisciplinary Sciences, Rensselaer Polytechnic Institute, Troy, New York 12180, United States;* orcid.org/0000-0002-2297-9219

Noah G. Allen − *Department of Biomedical Engineering and Center for Biotechnology and Interdisciplinary Sciences, Rensselaer Polytechnic Institute, Troy, New York 12180, United States*

Bhagyashree Subramaniam − *Department of Chemistry and Chemical Biology, Rensselaer Polytechnic Institute, Troy, New York 12180, United States; Center for Biotechnology and Interdisciplinary Sciences, Rensselaer Polytechnic Institute, Troy, New York 12180, United States*

Livia Carmody − *Department of Chemistry and Chemical Biology, Rensselaer Polytechnic Institute, Troy, New York 12180, United States*

Jonathan S. Dordick − *Department of Biomedical Engineering, Department of Chemical and Biological Engineering, and Center for Biotechnology and Interdisciplinary Sciences, Rensselaer Polytechnic Institute, Troy, New York 12180, United States;* orcid.org/0000-0001-7802-3702

David T. Corr − *Department of Biomedical Engineering, Rensselaer Polytechnic Institute, Troy, New York 12180, United States;* orcid.org/0000-0002-4059-8591

Complete contact information is available at: https://pubs.acs.org/10.1021/acsomega.3c09902

https://doi.org/10.1021/acsomega.3c09902
ACS Omega 2024, 9, 33408−33424

Author Contributions

MLC, RAG, and RTM conceptualized the overall synergy project. All biological assays were designed by RTM; data was collected with assistance from LC. Tumorigenic cells BT-474 were supplied by JSD; MDA-MB-231 and CCD1065SK cells were supplied by DTC. SEM imaging was completed by BS; FACS analysis was completed by NGA. Manuscript was written and edited by RTM; editing, data—review, and funding were done by RAG, MLC, DTC, and JSD.

Notes

The authors declare no competing financial interest.

■ ACKNOWLEDGMENTS

This research was funded by A24-0043 (R.A.G.), the National Institutes of Health (NIH) R01 CA233188 (D.T.C.), and NIGMS T32GM067545 (R.T.M.). We thank the Analytical Biochemistry Core, Flow Cytometry Core, and Scanning Electron Microscopy Core facilities at RPI for their equipment and advice in these biological assays.

■ REFERENCES

(1) Caesar, L. K.; Cech, N. B. Synergy and Antogonism in Natural Products. *Nat. Prod. Rep.* **2019**, *36* (5), 869.
(2) Hanson, M. A.; Dostálová, A.; Ceroni, C.; Poidevin, M.; Kondo, S.; Lemaitre, B. Synergy and Remarkable Specificity of Antimicrobial Peptides in Vivo Using a Systematic Knockout Approach. *Immunol. Inflammation* **2019**, *8*, No. e44341.
(3) Greve, J. M.; Cowan, J. A.; Greve, J. M. Tackling antimicrobial stewardship through synergy and antimicrobial peptides. *RSC Med. Chem.* **2022**, *13* (5), 511−521.
(4) Fouad, Y. A.; Aanei, C. Revisiting the Hallmarks of Cancer. *Am. J. Cancer Res.* **2017**, *7* (5), 1016.
(5) Ocana, A.; Amir, E.; Yeung, C.; Seruga, B.; Tannock, I. F. How Valid Are Claims for Synergy in Published Clinical Studies? *Ann. Oncol.* **2012**, *23* (8), 2161−2166.
(6) Chou, T. C. Drug Combination Studies and Their Synergy Quantification Using the Chou-Talalay Method. *Cancer Res.* **2010**, *70* (2), 440−446.
(7) Odds, F. C. Synergy, Antagonism, and What the Chequerboard Puts between Them. *J. Antimicrob. Chemother.* **2003**, *52* (1), 1.
(8) Castañeda, A. M.; Meléndez, C. M.; Uribe, D.; Pedroza-Díaz, J. Synergistic Effects of Natural Compounds and Conventional Chemotherapeutic Agents: Recent Insights for the Development of Cancer Treatment Strategies. *Heliyon* **2022**, *8* (6), No. e09519.
(9) Yuan, C. H.; Ma, Y. L.; Shih, P. C.; Chen, C. T.; Cheng, S. Y.; Pan, C. Y.; Jean, Y. H.; Chu, Y. M.; Lin, S. C.; Lai, Y. C.; Kuo, H. M. The Antimicrobial Peptide Tilapia Piscidin 3 Induces Mitochondria-Modulated Intrinsic Apoptosis of Osteosarcoma Cells. *Biochem. Pharmacol.* **2020**, *178*, 114064.
(10) Chen, W.; Cotten, M. L. Expression, Purification, and Micelle Reconstitution of Antimicrobial Piscidin 1 and Piscidin 3 for NMR Studies. *Protein Expression Purif.* **2014**, *102*, 63−68.
(11) Ting, C. H.; Chen, Y. C.; Wu, C. J.; Chen, J. Y. Targeting FOSB with a Cationic Antimicrobial Peptide, TP4, for Treatment of Triple-Negative Breast Cancer. *Oncotarget* **2016**, *7* (26), 40329−40347.
(12) Li, N.; Jiang, X.; Ma, X.; Qiu, X.; Chang, H. H.; Qiao, Y.; Luo, H.; Zhang, Q. Antimicrobial Peptides CS-Piscidin-Induced Cell Death Involves Activation of RIPK1/PARP, and Modification with Myristic Acid Enhances Its Stability and Tumor-Targeting Capability. *Discov. Oncol.* **2023**, *14* (1), 38.
(13) Comert, F.; Heinrich, F.; Chowdhury, A.; Schoeneck, M.; Darling, C.; Anderson, K. W.; Libardo, M. D. J.; Angeles-Boza, A. M.; Silin, V.; Cotten, M. L.; Mihailescu, M. Copper-Binding Anticancer Peptides from the Piscidin Family: An Expanded Mechanism That Encompasses Physical and Chemical Bilayer Disruption. *Sci. Rep.* **2021**, *11* (1), 12620.
(14) Chekmenev, E. Y.; Vollmar, B. S.; Forseth, K. T.; Manion, M. N.; Jones, S. M.; Wagner, T. J.; Endicott, R. M.; Kyriss, B. P.; Homem, L. M.; Pate, M.; He, J.; Raines, J.; Gor'kov, P. L.; Brey, W. W.; Mitchell, D. J.; Auman, A. J.; Ellard-Ivey, M. J.; Blazyk, J.; Cotten, M. Investigating Molecular Recognition and Biological Function at Interfaces Using Piscidins, Antimicrobial Peptides from Fish. *Biochim. Biophys. Acta, Biomembr.* **2006**, *1758* (9), 1359−1372.
(15) Libardo, M. D. J.; Bahar, A. A.; Ma, B.; Fu, R.; Mccormick, L. E.; Zhao, J.; Mccallum, S. A.; Nussinov, R.; Ren, D.; Angeles-boza, A. M.; et al. Nuclease Activity Gives an Edge to Host-Defense Peptide Piscidin 3 over Piscidin 1, Rendering It More Effective against Persisters and Biofilms. *FEBS J.* **2017**, *284*, 3662−3683.
(16) Kim, S. Y.; Zhang, F.; Gong, W.; Chen, K.; Xia, K.; Liu, F.; Gross, R.; Wang, J. M.; Linhardt, R. J.; Cotten, M. L. Copper Regulates the Interactions of Antimicrobial Piscidin Peptides from Fish Mast Cells with Formyl Peptide Receptors and Heparin. *J. Biol. Chem.* **2018**, *293*, 15381−15396.
(17) Comert, F.; Greenwood, A.; Maramba, J.; Acevedo, R.; Lucas, L.; Kulasinghe, T.; Cairns, L. S.; Wen, Y.; Fu, R.; Hammer, J.; Blazyk, J.; Sukharev, S.; Cotten, M. L.; Mihailescu, M. The Host-Defense Peptide Piscidin P1 Reorganizes Lipid Domains in Membranes and Decreases Activation Energies in Mechanosensitive Ion Channels. *J. Biol. Chem.* **2019**, *294* (49), 18557−18570.
(18) Chen, Y. F.; Shih, P. C.; Kuo, H. M.; Yang, S. N.; Lin, Y. Y.; Chen, W. F.; Tzou, S. J.; Liu, H. T.; Chen, N. F. TP3, an Antimicrobial Peptide, Inhibits Infiltration and Motility of Glioblastoma Cells via Modulating the Tumor Microenvironment. *Cancer Med.* **2020**, *9* (11), 3918−3931.
(19) Van Bogaert, I. N. A.; Saerens, K.; De Muynck, C.; Develter, D.; Soetaert, W.; Vandamme, E. J. Microbial Production and Application of Sophorolipids. *Appl. Microbiol. Biotechnol.* **2007**, *76* (1), 23−34.
(20) Peng, Y.; Totsingan, F.; Meier, M. A. R.; Steinmann, M.; Wurm, F.; Koh, A.; Gross, R. A. Sophorolipids: Expanding Structural Diversity by Ring-Opening Cross-Metathesis. *Eur. J. Lipid Sci. Technol.* **2015**, *117* (2), 217−228.
(21) Koh, A.; Todd, K.; Sherbourne, E.; Gross, R. A. Fundamental Characterization of the Micellar Self-Assembly of Sophorolipid Esters. *Langmuir* **2017**, *33* (23), 5760−5768.
(22) Sleiman, J. N.; Kohlhoff, S. A.; Roblin, P. M.; Wallner, S.; Gross, R.; Hammerschlag, M. R.; Zenilman, M. E.; Bluth, M. H. Sophorolipids as Antibacterial Agents. *Ann. Clin. Lab. Sci.* **2009**, *39* (1), 60−63.
(23) Jiménez-Peñalver, P.; Castillejos, M.; Koh, A.; Gross, R.; Sánchez, A.; Font, X.; Gea, T. Production and Characterization of Sophorolipids from Stearic Acid by Solid-State Fermentation, a Cleaner Alternative to Chemical Surfactants. *J. Cleaner Prod.* **2018**, *172*, 2735−2747.
(24) Ziemba, A. M.; Gottipati, M. K.; Totsingan, F.; Hanes, C. M.; Gross, R. A.; Lennartz, M. R.; Gilbert, R. J. Sophorolipid Butyl Ester Diacetate Does Not Affect Macrophage Polarization but Enhances Astrocytic Glial Fibrillary Acidic Protein Expression at Micromolar Concentrations in Vitro. *ACS Chem. Neurosci.* **2017**, *8* (4), 752−758.
(25) Totsingan, F.; Liu, F.; Gross, R. A. Structure-Activity Relationship Assessment of Sophorolipid Ester Derivatives against Model Bacteria Strains. *Molecules* **2021**, *26* (10), 3021.
(26) Dierickx, S.; Castelein, M.; Remmery, J.; De Clercq, V.; Lodens, S.; Baccile, N.; De Maeseneire, S. L.; Roelants, S. L. K. W.; Soetaert, W. K. From Bumblebee to Bioeconomy: Recent Developments and Perspectives for Sophorolipid Biosynthesis. *Biotechnol. Adv.* **2022**, *54*, 107788.
(27) Roberge, C. L.; Miceli, R. T.; Murphy, L. R.; Kingsley, D. M.; Gross, R. A.; Corr, D. T. Sophorolipid Candidates Demonstrate Cytotoxic Efficacy Against 2D And 3D Breast Cancer Models. *J. Nat. Prod.* **2023**, *86* (5), 1159−1170.
(28) Miceli, R. T.; Corr, D. T.; Barroso, M. M.; Dogra, N.; Gross, R. A. Sophorolipids: Anti-Cancer Activities and Mechanisms. *Bioorg. Med. Chem.* **2022**, *65*, 116787.

https://doi.org/10.1021/acsomega.3c09902
ACS Omega 2024, 9, 33408−33424

(29) Koh, A.; Gross, R. A. Molecular Editing of Sophorolipids by Esterification of Lipid Moieties: Effects on Interfacial Properties at Paraffin and Synthetic Crude Oil-Water Interfaces. *Colloids Surf., A* **2016**, *507*, 170−181.
(30) Koh, A.; Wong, A.; Quinteros, A.; Desplat, C.; Gross, R. Influence of Sophorolipid Structure on Interfacial Properties of Aqueous-Arabian Light Crude and Related Constituent Emulsions. *J. Am. Oil Chem. Soc.* **2017**, *94* (1), 107−119.
(31) Koh, A.; Linhardt, R. J.; Gross, R. Effect of Sophorolipid N-Alkyl Ester Chain Length on Its Interfacial Properties at the Almond Oil-Water Interface. *Langmuir* **2016**, *32* (22), 5562−5572.
(32) Joshi-Navare, K.; Shiras, A.; Prabhune, A. Differentiation-Inducing Ability of Sophorolipids of Oleic and Linoleic Acids Using a Glioma Cell Line. *Biotechnol. J.* **2011**, *6* (5), 509−512.
(33) Shao, L.; Song, X.; Ma, X.; Li, H.; Qu, Y.; Ph, D.; Ma, X.; Li, H.; Qu, Y.; Ph, D. Bioactivities of Sophorolipid with Different Structures against Human Esophageal Cancer Cells. *J. Surg. Res.* **2012**, *173* (2), 286.
(34) Ribeiro, I. A. C.; Faustino, C. M. C.; Guerreiro, P. S.; Frade, R. F. M.; Bronze, M. R.; Castro, M. F.; Ribeiro, M. H. L. Development of Novel Sophorolipids with Improved Cytotoxic Activity toward MDA-MB-231 Breast Cancer Cells. *J. Mol. Recognit.* **2015**, *28* (3), 155−165.
(35) Callaghan, B.; Lydon, H.; Roelants, S. L. K. W.; Van Bogaert, I. N. A.; Marchant, R.; Banat, I. M.; Mitchell, C. A. Lactonic Sophorolipids Increase Tumor Burden in Apcmin± Mice. *PLoS One* **2016**, *11* (6), No. e0156845.
(36) Sajid, M.; Ahmad Khan, M. S.; Singh Cameotra, S.; Safar Al-Thubiani, A. Biosurfactants: Potential Applications as Immunomodulator Drugs. *Immunol. Lett.* **2020**, *223*, 71−77.
(37) Bluth, M. H.; Kandil, E.; Mueller, C. M.; Shah, V.; Lin, Y. Y.; Zhang, H.; Dresner, L.; Nowakowski, M.; Lempert, L.; Gross, R.; Zenilman, M. E.; Schulze, R.; Lempert, L.; Nowakowski, M.; Nowakowski, M.; Schulze, R.; Zenilman, M. E. Sophorolipids Block Lethal Effects of Septic Shock in Rats in a Cecal Ligation and Puncture Model of Experimental Sepsis. *Crit. Care Med.* **2006**, *34* (1), 188.
(38) Diaz-Rodriguez, P.; Chen, H.; Erndt-Marino, J. D.; Liu, F.; Totsingan, F.; Gross, R. A.; Hahn, M. S. Impact of Select Sophorolipid Derivatives on Macrophage Polarization and Viability. *ACS Appl. Bio Mater.* **2019**, *2* (1), 601−612.
(39) Hardin, R.; Pierre, J.; Schulze, R.; Mueller, C. M.; Fu, S. L.; Wallner, S. R.; Stanek, A.; Shah, V.; Gross, R. A.; Weedon, J.; Nowakowski, M.; Zenilman, M. E.; Bluth, M. H. Sophorolipids Improve Sepsis Survival: Effects of Dosing and Derivatives. *J. Surg. Res.* **2007**, *142* (2), 314−319.
(40) Wang, G. S.; Chen, J. Y.; Chen, W. C.; Wei, I. C.; Lin, S. W.; Liao, K. W.; Yang, T. S.; Liu, J. F. Surfactin Induces ER Stress-Mediated Apoptosis via IRE1-ASK1-JNK Signaling in Human Osteosarcoma. *Environ. Toxicol.* **2022**, *37* (3), 574−584.
(41) Fu, S. L.; Wallner, S. R.; Bowne, W. B.; Hagler, M. D.; Zenilman, M. E.; Gross, R.; Bluth, M. H. Sophorolipids and Their Derivatives Are Lethal Against Human Pancreatic Cancer Cells. *J. Surg. Res.* **2008**, *148* (1), 77−82.
(42) Liu, F.; Greenwood, A. I.; Xiong, Y.; Miceli, R. T.; Fu, R.; Anderson, K. W.; Mccallum, S. A.; Mihailescu, M.; Gross, R.; Cotten, M. L. Host Defense Peptide Piscidin and Yeast-Derived Glycolipid Exhibit Synergistic Antimicrobial Action through Concerted Interactions with Membranes. *JACS Au* **2023**, *3*, 3345−3365.
(43) Scholz, C.; Mehta, S.; Bisht, V.; Guilmanov; Kaplan, D.; Nicolosi, R.; Gross, R. Bioactivity of Extracellular Glycolipids-Investigation of Potential Anti-Cancer Activity of Sophorolipids and Sophorolipid-Derivatives. *Polym. Prepr.* **1998**, *39*, 168.
(44) Lutter, A. H.; Scholka, J.; Richter, H.; Anderer, U. Applying XTT, WST-1, and WST-8 to Human Chondrocytes: A Comparison of Membrane-Impermeable Tetrazolium Salts in 2D and 3D Cultures. *Clin. Hemorheol. Microcirc.* **2017**, *67* (3−4), 327−342.
(45) *Cell Counting Kit WST- 8*. Sigma-Aldrich 2018; p 7.
(46) Jokar, F.; Mahabadi, J. A.; Salimian, M.; Taherian, A.; Hayat, S. M. G.; Sahebkar, A.; Atlasi, M. A.; Atlasi, M. A. Differential Expression of HSP90β in MDA-MB-231 and MCF-7 Cell Lines after Treatment with Doxorubicin. *J. Pharmacopuncture* **2019**, *22* (1), 28−34.
(47) Wen, S.-H.; Su, S.-C.; Liou, B.; Lin, C.; Lee, K. Sulbactam-Enhanced Cytotoxicity of Doxorubicin in Breast Cancer Cells. *Cancer Cell Int.* **2018**, *18* (1), 128.
(48) Miceli, R. T.; Corr, D. T.; Barroso, M.; Dogra, N.; Gross, R. A. Sophorolipids: Anti-Cancer Activities and Mechanisms. *Bioorg. Med. Chem.* **2022**, *65* (May), 116787.
(49) Lica, J. J.; Wieczór, M.; Grabe, G. J.; Heldt, M.; Jancz, M.; Misiak, M.; Gucwa, K.; Brankiewicz, W.; Maciejewska, N.; Stupak, A.; Bagiński, M.; Rolka, K.; Hellmann, A.; Składanowski, A. Effective Drug Concentration and Selectivity Depends on Fraction of Primitive Cells. *Int. J. Mol. Sci.* **2021**, *22* (9), 4931.
(50) Indo, H. P.; Yen, H. C.; Nakanishi, I.; Matsumoto, K. I.; Tamura, M.; Nagano, Y.; Matsui, H.; Gusev, O.; Cornette, R.; Okuda, T.; Minamiyama, Y.; Ichikawa, H.; Suenaga, S.; Oki, M.; Sato, T.; Ozawa, T.; Clair, D. K. S.; Majima, H. J. A Mitochondrial Superoxide Theory for Oxidative Stress Diseases and Aging. *J. Clin. Biochem. Nutr.* **2015**, *56* (1), 1−7.
(51) Hadji, A.; Ceppi, P.; Murmann, A. E.; Brockway, S.; Pattanayak, A.; Bhinder, B.; Hau, A.; De Chant, S.; Parimi, V.; Kolesza, P.; Richards, J. A.; Chandel, N.; Djaballah, H.; Peter, M. E. Death Induced by CD95 or CD95 Ligand Elimination. *Cell Rep.* **2014**, *7* (1), 208−222.
(52) Brentnall, M.; Rodriguez-Menocal, L.; De Guevara, R. L.; Cepero, E.; Boise, L. H. Caspase-9, Caspase-3 and Caspase-7 Have Distinct Roles during Intrinsic Apoptosis. *BMC Cell Biol.* **2013**, *14* (1), 32.
(53) Cao, X. H.; Zhao, S. S.; Liu, D. Y.; Wang, Z.; Niu, L. L.; Hou, L. H.; Wang, C. L. ROS-Ca2+ Is Associated with Mitochondria Permeability Transition Pore Involved in Surfactin-Induced MCF-7 Cells Apoptosis. *Chem.-Biol. Interact.* **2011**, *190* (1), 16−27.
(54) Perillo, B.; Di Donato, M.; Pezone, A.; Di Zazzo, E.; Giovannelli, P.; Galasso, G.; Castoria, G.; Migliaccio, A. ROS in Cancer Therapy: The Bright Side of the Moon. *Exp. Mol. Med.* **2020**, *52* (2), 192−203.
(55) Leshem, Y.; Melamed-Book, N.; Cagnac, O.; Ronen, G.; Nishri, Y.; Solomon, M.; Cohen, G.; Levine, A. Suppression of *Arabidopsis* vesicle-SNARE expression inhibited fusion of H_2O_2-containing vesicles with tonoplast and increased salt tolerance. *Plant Signaling Behav.* **2006**, *103* (47), 18008−18013.
(56) Cao, S. S.; Kaufman, R. J. Endoplasmic Reticulum Stress and Oxidative Stress in Cell Fate Decision and Human Disease. *Antioxid. Redox Signaling* **2014**, *21* (3), 396−413.
(57) Brand, M. D.; Orr, A. L.; Perevoshchikova, I. V.; Quinlan, C. L. The Role of Mitochondrial Function and Cellular Bioenergetics in Ageing and Disease. *Br. J. Dermatol.* **2013**, *169*, 1−8.
(58) Boland, M. L.; Chourasia, A. H.; Macleod, K. F. Mitochondrial Dysfunction in Cancer. *Front. Oncol.* **2013**, *3* (292), 1−28.
(59) Wang, C.; Youle, R. J. The Role of Mitochondria in Apoptosis. *Annu. Rev. Genet.* **2009**, *43*, 95−118.
(60) Dai, X.; Cheng, H.; Bai, Z.; Li, J. Breast Cancer Cell Line Classification and Its Relevance with Breast Tumor Subtyping. *J. Cancer* **2017**, *8* (16), 3131−3141.
(61) Robinson, M. A.; Graham, D. J.; Morrish, F.; Hockenbery, D.; Gamble, L. J. Lipid Analysis of Eight Human Breast Cancer Cell Lines with ToF-SIMS. *Biointerphases* **2016**, *11* (2), 02A303.
(62) Vultaggio-Poma, V.; Sarti, A. C.; Di Virgilio, F. Extracellular ATP: A Feasible Target for Cancer Therapy. *Cells* **2020**, *9* (11), 2496.
(63) Op den Kamp, J. A. F. Lipid Asymmetry in Membranes. *Annu. Rev. Biochem.* **1979**, *48*, 47−71.
(64) Koopman, G.; Reutelingsperger, C. P. M.; Kuijten, G. A. M.; Keehnen, R. M. J.; Pals, S. T.; van Oers, M. Annexin V for Flow Cytometric Detection of Phosphatidylserine Expression on B Cells Undergoing Apoptosis. *Blood* **1994**, *84* (5), 1415−1420.
(65) Thiagarajan, P.; Tait, J. F. Binding of annexin V/placental anticoagulant protein I to platelets. Evidence for phosphatidylserine exposure in the procoagulant response of activated platelets. *J. Biol. Chem.* **1990**, *265*, 17420−17423.

https://doi.org/10.1021/acsomega.3c09902
ACS Omega 2024, 9, 33408−33424

(66) Shlomovitz, I.; Speir, M.; Gerlic, M. Flipping the Dogma - Phosphatidylserine in Non-Apoptotic Cell Death. *Cell Commun. Signaling* **2019**, *17* (1), 139.
(67) Brouckaert, G.; Kalai, M.; Krysko, D. V.; Saelens, X.; Vercammen, D.; Ndlovu, M.; Haegeman, G.; D'Herde, K.; Vandenabeele, P. Phagocytosis of Necrotic Cells by Macrophages Is Phosphatidylserine Dependent and Does Not Induce Inflammatory Cytokine Production. *Mol. Biol. Cell* **2004**, *15*, 1089−1100.
(68) Gong, Y.-N.; Guy, C.; Olauson, H.; Becker, J. U.; Yang, M.; Fitzgerald, P.; Linkermann, A.; Green, D. R. ESCRT-III Acts Downstream of MLKL to Regulate Necroptotic Cell Death and Its Consequences. *Cell* **2017**, *169* (2), 286.
(69) de Vasconcelos, N. M.; Van Opdenbosch, N.; Van Gorp, H.; Parthoens, E.; Lamkanfi, M. Single-Cell Analysis of Pyroptosis Dynamics Reveals Conserved GSDMD-Mediated Subcellular Events That Precede Plasma Membrane Rupture. *Cell Death Differ.* **2019**, *26* (1), 146−161.
(70) Yang, J.; Hu, S.; Bian, Y.; Yao, J.; Wang, D.; Liu, X.; Guo, Z.; Zhang, S.; Peng, L. Targeting Cell Death: Pyroptosis, Ferroptosis, Apoptosis and Necroptosis in Osteoarthritis. *Front. Cell Dev. Biol.* **2022**, *9*, 1−18.
(71) Klöditz, K.; Fadeel, B. Three Cell Deaths and a Funeral: Macrophage Clearance of Cells Undergoing Distinct Modes of Cell Death. *Cell Commun. Signaling* **2019**, *5* (65), 65.
(72) Le Gallo, M.; Poissonnier, A.; Blanco, P.; Legembre, P. CD95/Fas, Non-Apoptotic Signaling Pathways, and Kinases. *Front. Immunol.* **2017**, *8*, 1216.
(73) Lynch, D. H.; Campbell, K. A.; Miller, R.; Bradley, A.; Paya, C. FasL/Fas and TNF/TNFR Interactions in the Regulation of Immune Responses and Disease. *Behring Inst. Mitt.* **1996**, *97*, 175−184.
(74) Peter, M. E.; Hadji, A.; Murmann, A. E.; Brockway, S.; Putzbach, W.; Pattanayak, A.; Ceppi, P. The Role of CD95 and CD95 Ligand in Cancer. *Cell Death Differ.* **2015**, *22* (4), 549−559.
(75) Buhling, F.; Wille, A.; Rocken, C.; Wiesner, O.; Baier, A.; Meinecke, I.; Welte, T.; Pap, T. Altered Expression of Membrane-Bound and Soluble CD95/Fas Contributes to the Resistance of Fibrotic Lung Fibroblasts to FasL Induced Apoptosis. *Respir. Res.* **2005**, *6*, 37.
(76) Sejima, T.; Miyagawa, I. Significance of Fas Expression Alteration during Tumor Progression of Renal Cell Carcinoma. *Int. J. Urol.* **2006**, *13*, 257−264.
(77) Hardwick, J. M.; Soane, L. Multiple Functions of BCL-2 Family Proteins. *Cold Spring Harbor Perspect. Biol.* **2013**, *5* (2), a008722.
(78) Tanida, I.; Minematsu-Ikeguchi, N.; Ueno, T.; Kominami, E. Lysosomal Turnover, but Not a Cellular Level, of Endogenous LC3 Is a Marker for Autophagy. *Autophagy* **2005**, *1* (2), 84−91.
(79) Warren, C. F. A.; Wong-Brown, M. W.; Bowden, N. A. BCL-2 Family Isoforms in Apoptosis and Cancer. *Cell Death Dis.* **2019**, *10* (3), 177.
(80) Celli, A.; Que, F. G.; Gores, G. J.; LaRusso, N. F. Glutathione Depletion Is Associated with Decreased Bcl-2 Expression and Increased Apoptosis in Cholangiocytes. *Am. J. Physiol.: Gastrointest. Liver Physiol.* **1998**, *275* (4), 749−757.
(81) Liu, T.; Wu, Z.; He, Y.; Xiao, Y.; Xia, C. Single and Dual Target Inhibitors Based on Bcl-2: Promising Anti-Tumor Agents for Cancer Therapy. *Eur. J. Med. Chem.* **2020**, *201* (112446), 112446.
(82) Trocoli, A.; Djavaheri-Mergny, M. The Complex Interplay between Autophagy and NF-KB Signaling Pathways in Cancer Cells. *Am. J. Cancer Res.* **2011**, *1* (5), 629−649.
(83) Pavlova, N. N.; Zhu, J.; Thompson, C. B. The Hallmarks of Cancer Metabolism: Still Emerging. *Cell Metab.* **2022**, *34* (3), 355−377.
(84) Kumar, M.; Irungbam, K.; Kataria, M. Depletion of Membrane Cholesterol Compromised Caspase-8 Imparts in Autophagy Induction and Inhibition of Cell Migration in Cancer Cells. *Cancer Cell Int.* **2018**, *18* (1), 23.
(85) Balleza, D.; Alessandrini, A.; Beltrán García, M. J. Role of Lipid Composition, Physicochemical Interactions, and Membrane Mechanics in the Molecular Actions of Microbial Cyclic Lipopeptides. *J. Membr. Biol.* **2019**, *252* (2−3), 131−157.
(86) Wójtowicz, K.; Czogalla, A.; Trombik, T.; Łukaszewicz, M. Surfactin Cyclic Lipopeptides Change the Plasma Membrane Composition and Lateral Organization in Mammalian Cells. *Biochim. Biophys. Acta, Biomembr.* **2021**, *1863* (12), 183730.
(87) Vona, R.; Iessi, E.; Matarrese, P. Role of Cholesterol and Lipid Rafts in Cancer Signaling: A Promising Therapeutic Opportunity? *Front. Cell Dev. Biol.* **2021**, *9*, 1−19.
(88) Zhang, Y.; Chen, X.; Gueydan, C.; Han, J. Plasma Membrane Changes during Programmed Cell Deaths. *Cell Res.* **2018**, *28* (1), 9−21.
(89) Fang, Y.; Tian, S.; Pan, Y.; Li, W.; Wang, Q.; Tang, Y.; Yu, T.; Wu, X.; Shi, Y.; Ma, P.; Shu, Y. Pyroptosis: A New Frontier in Cancer. *Biomed. Pharmacother.* **2020**, *121*, 109595.
(90) Ivascu, A.; Kubbies, M. Diversity of Cell-Mediated Adhesions in Breast Cancer Spheroids. *Int. J. Oncol.* **2007**, *31* (6), 1403−1413.
(91) Le, W.; Chen, B.; Cui, Z.; Liu, Z.; Shi, D. Detection of Cancer Cells Based on Glycolytic-Regulated Surface Electrical Charges. *Biophys. Rep.* **2019**, *5* (1), 10−18.
(92) Szlasa, W.; Zendran, I.; Zalesinska, A.; Tarek, M.; Kulbacka, J. Lipid Composition of the Cancer Cell Membrane. *J. Bioenergics Biomembr.* **2020**, *52*, 321−342.
(93) Vallabhapurapu, S. D.; Blanco, V. M.; Sulaiman, M. K.; Vallabhapurapu, S. L.; Chu, Z.; Franco, R. S.; Qi, X. Variation in Human Cancer Cell External Phosphatidylserine Is Regulated by Flippase Activity and Intracellular Calcium. *Oncotarget* **2015**, *6* (33), 34375−34388.
(94) Nawale, L.; Dubey, P.; Chaudhari, B.; Sarkar, D.; Prabhune, A. Anti-Proliferative Effect of Novel Primary Cetyl Alcohol Derived Sophorolipids against Human Cervical Cancer Cells HeLa. *PLoS One* **2017**, *12* (4), No. e0174241.
(95) Li, H.; Guo, W.; Ma, X. j.; Li, J. s.; Song, X. In Vitro and in Vivo Anticancer Activity of Sophorolipids to Human Cervical Cancer. *Appl. Biochem. Biotechnol.* **2017**, *181* (4), 1372−1387.
(96) Cheng, M.-H.; Pan, C. Y.; Chen, N. F.; Yang, S. N.; Hsieh, S.; Wen, Z. H.; Chen, W. F.; Wang, J. W.; Lu, W. H.; Kuo, H. M. Piscidin-1 Induces Apoptosis via Mitochondrial Reactive Oxygen Species-Regulated Mitochondrial Dysfunction in Human Osteosarcoma Cells. *Sci. Rep.* **2020**, *10* (1), 5045.
(97) Shrestha, A. *Study of Piscidin 1 in Models of Cancer Cell Membranes and Healthy Mammalian Cell Membranes*; Hamilton College, 2013.
(98) Marquez, R. T.; Xu, L. Bcl-2:Beclin 1 Complex: Multiple, Mechanisms Regulating Autophagy/Apoptosis Toggle Switch. *Am. J. Cancer Res.* **2012**, *2* (2), 214−221.
(99) Prerna, K.; Dubey, V. K. Beclin1-Mediated Interplay between Autophagy and Apoptosis: New Understanding. *Int. J. Biol. Macromol.* **2022**, *204*, 258−273.
(100) Qian, M.; Fang, X.; Wang, X. Autophagy and Inflammation. *Clin. Transl. Med.* **2017**, *6* (1), No. e24.
(101) Ricci, M. S.; Zong, W.-X. Chemotherapeutic Approaches for Targeting Cell Death Pathways. *Oncologist* **2006**, *11* (4), 342−357.
(102) Yan, G.; Elbadawi, M.; Efferth, T. Multiple Cell Death Modalities and Their Key Features (Review). *World Acad. Sci. J.* **2020**, *2* (2), 39−48.
(103) Rambold, A. S.; Lippincott-Schwartz, J. Mechanisms of Mitochondria and Autophagy Crosstalk. *Cell Cycle* **2011**, *10* (23), 4032−4038.
(104) Wang, S.; Liu, Y.; Zhang, L.; Sun, Z. Methods for Monitoring Cancer Cell Pyroptosis. *Cancer Biol. Med.* **2021**, *19* (4), 398−414.
(105) Chen, Q.; Kang, J.; Fu, C. The Independence of and Associations among Apoptosis, Autophagy, and Necrosis. *Signal Transduction Targeted Ther.* **2018**, *3* (1), 18.
(106) Peter, M. E.; Krammer, P. H. The CD95(APO-1/Fas) DISC and Beyond. *Cell Death Differ.* **2003**, *10* (1), 26−35.
(107) Lee, S.; Shanti, A. Effect of Exogenous pH on Cell Growth of Breast Cancer Cells. *Int. J. Mol. Sci.* **2021**, *22* (18), 9910.

https://doi.org/10.1021/acsomega.3c09902
ACS Omega 2024, 9, 33408−33424

(108) Chekmenev, E. Y.; Jones, S. M.; Nikolayeva, Y. N.; Vollmar, B. S.; Wagner, T. J.; Gor'kov, P. L.; Brey, W. W.; Manion, M. N.; Daugherty, K. C.; Cotten, M. High-Field NMR Studies of Molecular Recognition and Structure - Function Relationships in Antimicrobial Piscidins at the Water - Lipid Bilayer Interface. *JACS Commun.* **2006**, *128*, 5308−5309.
(109) Oludiran, A.; Courson, D. S.; Stuart, M. D.; Radwan, A. R.; Poutsma, J. C.; Cotten, M. L.; Purcell, E. B. How Oxygen Availability Affects the Antimicrobial Efficacy of Host Defense Peptides: Lessons Learned from Studying the Copper-Binding Peptides Piscidins 1 and 3. *Int. J. Mol. Sci.* **2019**, *20* (21), 5289.
(110) Promega Corporation *Mitochondrial ToxGlo Assay: Instructions for Use of Products G8000 and G8001*; Promega, 2011; pp 1−18.
(111) Molecular Probes *CellROX Oxidative Stress Reagents*; Life Technologies, 2012; pp 1−6.
(112) Invitrogen *Violet Annexin V/Dead Cell Apoptosis Kit with Pacific Blue Annexin V/SYTOX AADvanced for Flow Cytometry*; Thermo Fisher Scientific, 2009; pp 1−5.
(113) Invitrogen. MitoSOX Red Mitochondrial Superoxide Indicator; Thermo Fisher Scientific, 2022; pp 1−2.
(114) Guide, U. *Human SAPO-1/Fas ELISA Kit*; Biovendar; pp 1−7.
(115) Cell BioLabs *Autophagy ELISA Kit (LC3-II Quantitation)*; Cell BioLabs, Inc., 2022; pp 1−10.
(116) Invitrogen *Amplex Red Cholesterol Assay Kit*; Molecular Probes, 2010; pp 1−6.

https://doi.org/10.1021/acsomega.3c09902
ACS Omega 2024, 9, 33408−33424